Non-destructive inspection technologies for repair assessment in materials and structures

Developments in the Built Environment 18 (2024) 100443

Contents lists available at ScienceDirect

Developments in the Built Environment

journal homepage: www.sciencedirect.com/journal/developments-in-the-built-environment

# Non-destructive inspection technologies for repair assessment in materials and structures

T. Shiotani [a], N. Ogura [a], N. Okude [a], K. Watabe [a,b], C. Van Steen [c], E. Tsangouri [d,e], G. Lacidogna [f], S. Czarnecki [g], H.K. Chai [h], Y. Yang [i], E. Verstrynge [c], D.G. Aggelis [d,*]

[a] Department of Civil and Earth Resources Engineering, Graduate School of Engineering, Kyoto University, Kyoto, Japan
[b] Research and Development Center, Toshiba Corp, Kawasaki, Japan
[c] Department of Civil Engineering, Materials and Constructions Division, KU Leuven, Leuven, Belgium
[d] Department of Mechanics of Materials and Constructions, Vrije Universiteit Brussel (VUB), Brussels, Belgium
[e] CY Cergy Paris Université, Laboratoire de Mécanique et Matériaux du Génie Civil (L2MGC), Neuville-sur-Oise, France
[f] Department of Structural, Geotechnical and Building Engineering, Politecnico di Torino, Torino, Italy
[g] Faculty of Civil Engineering, Wroclaw University of Science and Technology, Wroclaw, Poland
[h] School of Engineering, The University of Edinburgh, Edinburgh, United Kingdom
[i] Department of Engineering Structures, Delft University of Technology, the Netherlands

ARTICLE INFO

*Keywords:*
Repair
Concrete
Cement
Masonry
Ultrasound
NDT
Acoustic emission (AE)
Digital image correlation (DIC)
RILEM TC 269-IAM

ABSTRACT

Aging infrastructure globally faces degradation, posing risks and requiring substantial repair investment. Strategic maintenance practices are crucial for evaluating structural conditions and ensuring sustainability. The growing demands on modern materials and structures necessitate enhanced health monitoring approaches. Shifting from reactive to proactive maintenance methodologies is paramount, due to lower investment while keeping the structural performance at acceptable standards. However, quantitative assurance of repair/reinforcement/retrofit programs or self-healing effect in structures is similarly crucial for the operation of the infrastructure. Non-destructive testing (NDT) techniques, such as ultrasound, acoustic emission, and optical methods, play a vital role in assessing structural health. Through real-world case studies, the effectiveness of repair in addition to damage assessment are evaluated, encouraging a more systematic approach to monitoring structural repair efficacy. The paper intends to address the research gap in monitoring the repair effectiveness in civil structures and materials and provides valuable insights to enhance repair strategies in civil engineering.

## 1. Introduction

The increasing international interest in environmental conservation, sustainability, carbon dioxide reduction and structural safety leads to a mounting desire to extend the service life of existing structures (Silfwerbrand, 2009). Therefore, repair gains higher priority in budget allocations for civil engineering works, and the resort to repair is often also motivated by the tight global economic conditions. Failing to recognize early signs of damage leads to a multiplication of costs by a factor of 25 when the operation of the structure becomes troublesome and extensive repair is required (Delatte, 2009). It is indicative that the global repair mortar market is continuously increasing, projected to grow to USD 4 billion by 2026 (Markets and Markets, 2024). Despite its continuously increasing importance, there is a lack of attention on repair of structures in the engineering curricula, even though in many cases aging infrastructure needs urgent measures to be reinstated to normal operational condition. The objectives of repair include restoration of strength and stiffness, improvement of durability and operational performance, among other specific benefits such as providing watertightness or conserving the aesthetics of structures. Repair in different forms can be performed and, when properly conducted, can substantially increase the life span of the structures, saving resources in raw building materials, capital, working hours, and eliminate the problems of construction waste disposal and recycling. However, a crucial point is that the effectiveness of repair should be examined in order to validate the restoration of properties or that it has fulfilled the initial intervention purpose. Due to the heterogeneity on structures design and material usage, effective restoration is not always a straightforward task. In most

* Corresponding author.
*E-mail address:* Dimitrios.Aggelis@vub.be (D.G. Aggelis).

https://doi.org/10.1016/j.dibe.2024.100443
Received 12 March 2024; Received in revised form 24 April 2024; Accepted 24 April 2024
Available online 27 April 2024

cases, visual inspection for the validation of an effective intervention would not suffice the requirements, as for example when repair agent is injected into the cracks, or when an external patch is bonded on an existing surface. For all above reasons, quantification of the repair effectiveness is important for strategizing long-term and efficient construction usage. The increasing need for accurate information and management of structures is showcased by the rapid increase of the structural health monitoring (SHM) market which is projected to overpass USD 5 billion by 2030 (Global Structural Health Monitoring, 2021).

This article aims to provide an overview on key monitoring technologies that can be eventually applied in-situ, thus are non-destructive in nature, to evaluate the effectiveness of structural repair. This is a contemporary topic treated by RILEM Technical Committee (TC) 269-IAM (RILEM TC 269-IAM, 2023). The article is organized based on the different repair technologies and the NDT methods that are (or can be) applied for repair validation and could also be applied for initial damage state assessment. A short introduction of the basic principles of each technique is given in each corresponding section that follows. The main identified repair technologies for concrete and masonry structures are injection into individual cracks, bonding of external patch and external layers in general, as well as the triggering of autogenous and autonomous healing.

## 2. Concrete repair

Despite the several advantages of (reinforced) concrete technology in the last century, the material remains until today sensitive, among others, to tensile stresses and durability loss. Given that concrete structures are built to last for several decades, it is understandable that repair and maintenance interventions will most likely be necessary to ensure safe use and to extend the service life.

### 2.1. Repair by injection-grouting

#### 2.1.1. Through the thickness evaluation

In this case, a filling material is placed (injected by pressure and with the aid of capillary action) into the cracked volume. This can be applied through the opening of surface breaking cracks using syringes that push liquid agent (commonly epoxy) into the empty volume of the crack (Issa, 2009, Fig. 1(a)). Alternatively, a certain predefined grid is prepared by drilling holes and injecting cementitious grout into the structure (Fig. 1 (b)).

Due to the interconnected nature of cracks and inherent porosity, especially in heavily damaged cases, the pressurized liquid can penetrate into a significant part of the cracked volume, eliminating these voids. Filling the voids and sealing the cracks, increases the loadbearing capacity of the damaged cross-section. The volume of the injected material can be controlled and quantitatively measured. However, the volume of the crack or the crack network that has been eventually filled cannot be known a priori. Therefore, assessment must be done from the surface and requires information from the interior of the structure. In this case, elastic waves have proven very useful. Apart from their non-invasive nature, their advantage is that they physically propagate through the material and therefore, collect information on the elastic modulus and density of the constituents. In a three-dimensional wave propagation case, the velocity C, of longitudinal waves is connected to the elastic modulus $E$, the density $\rho$, and the Poisson's ratio $\nu$, through the following fundamental relation (Naik et al., 2003):

$$C = \sqrt{\frac{E(1-\nu)}{\rho(1+\nu)(1-2\nu)}} \tag{1}$$

Elastic waves propagate through solid media like concrete with velocities of the order of 4000 m/s in an intact state. At the same time, when damage is included in the path, the propagation is much slower, and the transmission is reduced due to attenuation. Therefore, variations in the wave velocity can be used to demonstrate the stiffness of the propagation path and its general condition (Ahn et al., 2017; Chaix et al., 2006).

In case of specific defects like through-thickness cracks in a concrete slab, ultrasonic wave propagation and tracking could successfully evaluate the difference between the damaged and the repaired state of the member after epoxy injection. In Aggelis and Shiotani (2007), groups of five resonant piezoelectric sensors were arranged at the top and the bottom surface, Fig. 2(a). Excitations were made at each sensor position and the propagating wave was recorded at all other sensor positions. Reasonably, wave paths not intersected by the crack exhibited higher velocity than the ones including a crack. By combining the information of the transit time of all the different wave paths in the tomography procedure, the visualization of the velocity structure of the cross-section is conducted (see Fig. 2(b)). In the initial tomogram, the crack is clearly visible, and associated with much lower wave velocity than the sound material away from the crack. After repair, the overall velocity map has substantially improved since the void was filled. In Fig. 2(c), there are only tiny traces of the crack still visible, something considered normal because the epoxy, even though it has higher strength than concrete, possesses a lower elastic modulus (3–5 GPa). Nevertheless, the information supplied by the ultrasonic tomogram was sufficient to realize that the filling was satisfactory and allowed the continuation of the works.

In another case accelerometers were installed, and elastic waves were used to evaluate, not specific cracks, but the overall damage

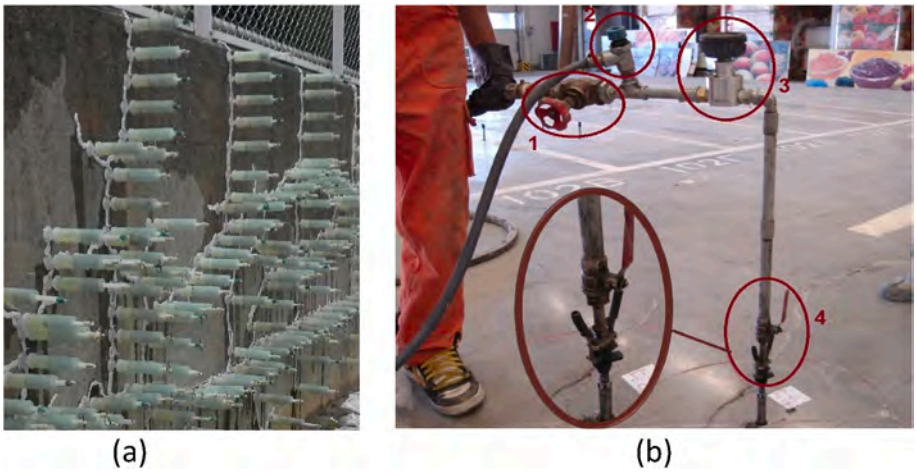


**Fig. 1.** (a) Epoxy injection in a concrete wall (courtesy Kyoto University) and (b) grouting injection in a concrete floor (Zoidis et al., 2013).

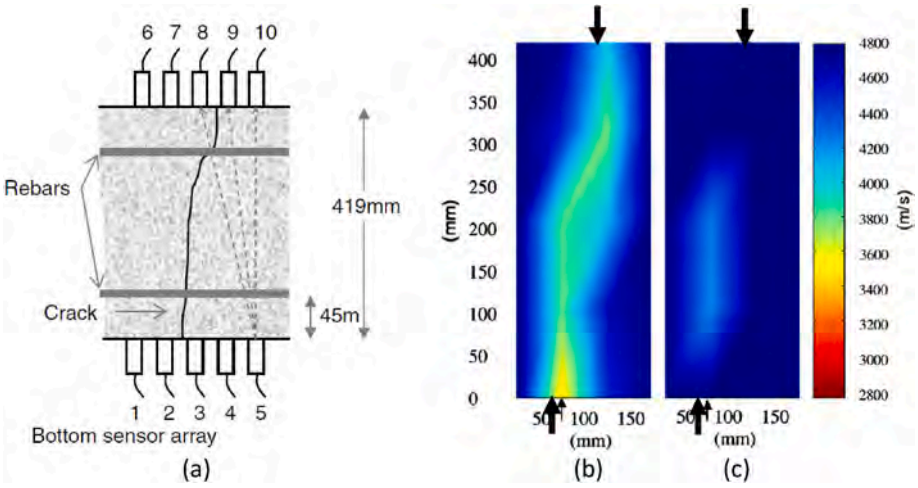


**Fig. 2.** (a) Side view of the sensor locations and crack position through the bridge deck, (b) ultrasonic tomogram before repair, and (c) after repair with epoxy injection in the crack (Aggelis and Shiotani, 2007).

condition and the repair effectiveness of grouting (through a certain predefined grid) in pylons of a water intake facility (Shiotani et al., 2009). The final modulus of the cementitious grout was nominally 21.5 GPa, while the one of the original concrete was evaluated at 35 GPa. After grouting was performed and allowing the necessary curing period, through-thickness elastic wave testing was conducted (Fig. 3(a)) and compared to the results of the reference investigation before repair. The excitation was conducted with a pneumatic impact hammer, and low frequency accelerometers (up to 40 kHz) were used to capture the response from opposite sides of the structure. Low frequencies were necessary due to the large size and long propagation distances, while stacking of approximately 800 individual excitations was also applied to enhance the signal-to-noise ratio of the waveforms. Combining the transit time of all different wave paths, tomography results showed the distribution of reference damage (Fig. 3(b)), while after injection and hardening of the grout (Fig. 3(c)), there was an overall velocity increase of approximately 5–10 % (Shiotani et al., 2009), with specific regions showing greater or limited restoration.

As a side note, the final results of elastic wave measurement and the associated tomographic reconstruction were obtained after complete hardening of the grout material while the improvement was not evident through the wave velocity structure immediately after the injection work which occurred under cold conditions. A theoretical elastic wave study revealed that the reason is a combination of the initial low stiffness of the grout, the low hardening rate in cold environment and the low excitation frequencies (approximately 10 kHz) (Shiotani et al., 2009). In addition, it was verified experimentally, that specimens of porous concrete after impregnation with repairing grout exhibited an initial decrease of wave velocity when maintained at low temperatures (5°C) in contrast to (20°C) that showed immediate increase (Aggelis and Shiotani, 2009a). This indicates that although repair through injection can physically fill voids, it should not be immediately expected to reflect on the wave velocity increase. This is particularly important for repair cases under cold conditions, which would delay the curing and stiffness realization of the filling material.

In an extended work at the same water intake facility which required validation of the repair effectiveness of other concrete pylons, three-dimensional elastic wave tomography was developed and applied (Momoki et al., 2013). For measuring the elastic waves' travel time, 48 accelerometers with a maximum frequency of 40 kHz, as in the above case, were instrumented on three sides of each pylon as shown in Fig. 4 (a). The arrangement created altogether 1512 potential "ray paths" for elastic wave through-the-thickness transmissions, as indicated in Fig. 4 (b). The longest straight-line distance between two accelerometers was 9.7 m. Elastic waves were excited by two different mechanical means: manual steel ball hammer impact and electro-pneumatic hammer impact to cater for comparison purpose on the effectiveness of signal generation and acquisition. The travel time tomography results are exemplified in Fig. 5(a) from measuring one of the pylons. The three-dimensional tomographic reconstruction has allowed for the visualization of any cross sections (i.e. Fig. 5(b)) of interest internally without the need to repeat measurements. This feature further adds to the technique's versatility for use in evaluating the repair efficiency of materials and structures of practical scales.

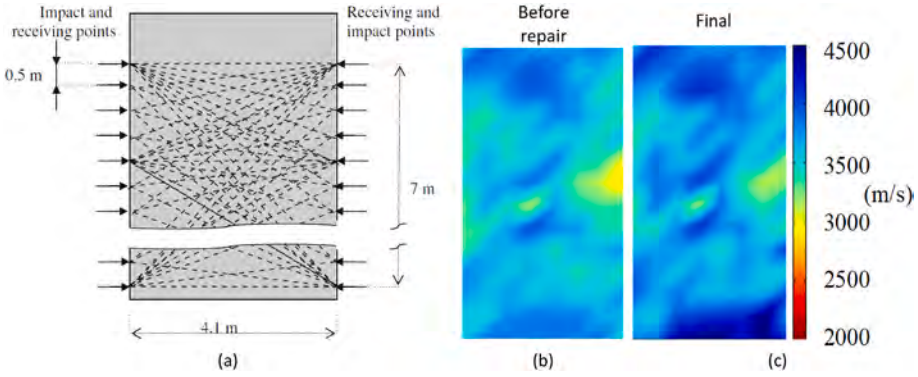


**Fig. 3.** (a) Schematic representation of concrete cross section with elastic wave paths, (b) wave velocity tomograms before and (c) after repair through grout injection (Shiotani et al., 2009).

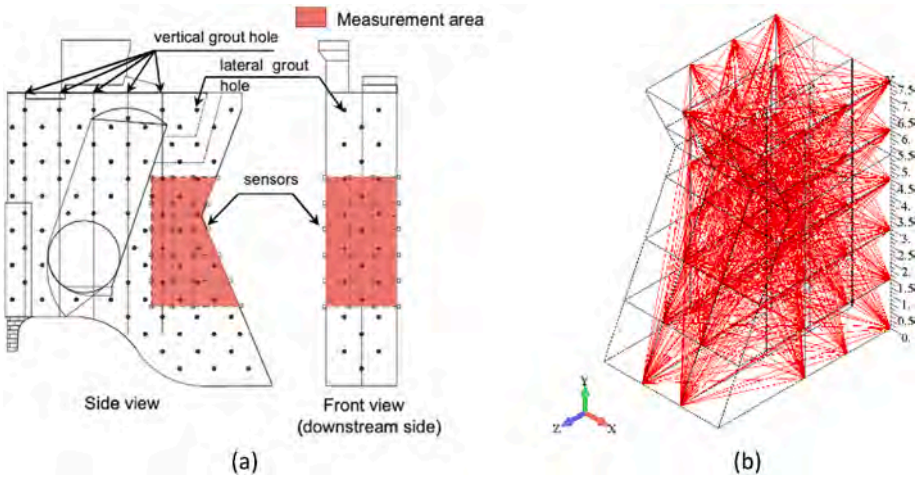


**Fig. 4.** Application of three-dimensional elastic wave tomography: (a) accelerometer placement, (b) ray path distribution (Momoki et al., 2013).

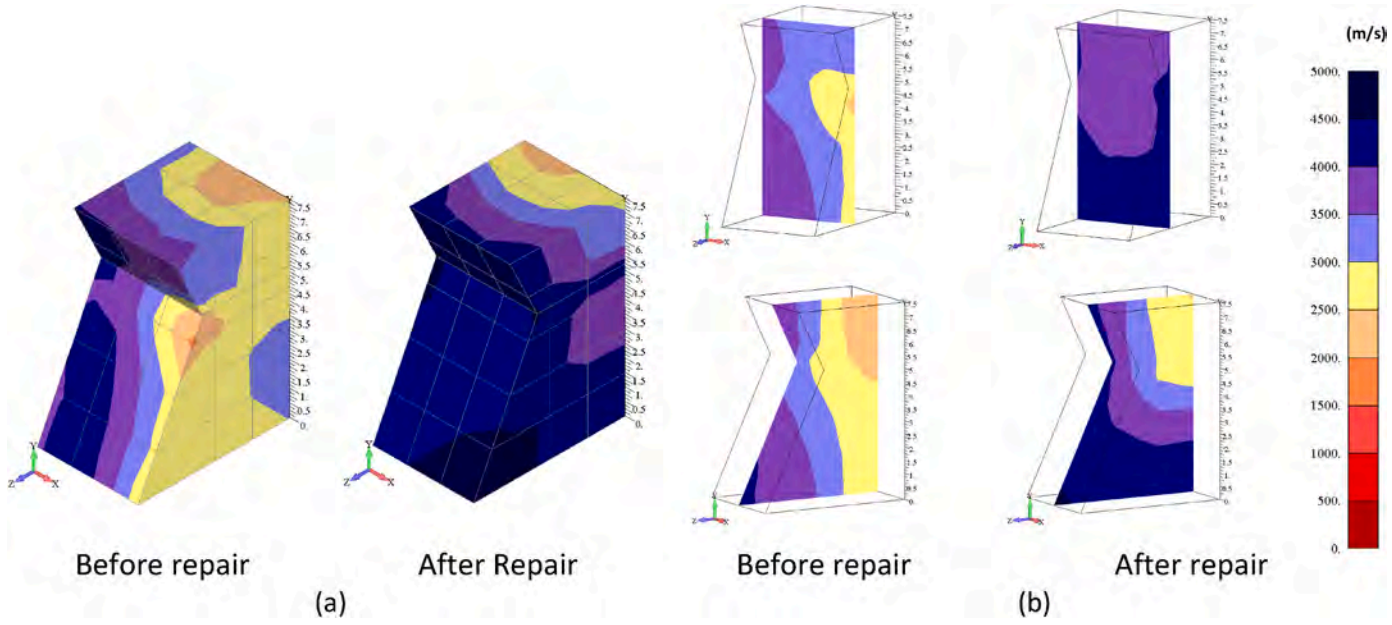


**Fig. 5.** Elastic wave tomographic reconstruction results of concrete pylon: (a) three-dimensional coverage, (b) central cross section visualizations (Momoki et al., 2013).

For the same structure (the pylons of water intake facility), the acoustic emission (AE) technique was also applied during water pressurization tests in drilled boreholes. Piezoelectric AE sensors were applied on the structure's surface recording any transient elastic wave during pressurization of the material, which is usually due to microcracking. AE is very sensitive to the onset of cracking under applied load (Grosse et al., 2022). In this specific case, the water pressure was increased in a controlled way and the piezoelectric AE sensors on the external surfaces as well as the sensors attached to waveguides inside the structure recorded the emissions. The test took place before and after repair and AE indices revealed the restoration of material integrity. Practically, after repair, for the same water pressure much less AE signals were recorded, verifying that a large amount of interconnected pores or capillaries were sealed, showing the positive effect of repair (Shiotani and Aggelis, 2007). This was measured by the Felicity ratio (Fowler, 1977), which quantified the delay of the AE onset after repair.

Another example of elastic wave velocity tomography comes from a reinforced concrete structure (Sagradyan et al., 2023). The construction in this case is a complex process, consisting of formwork installation, reinforcement placement, concrete casting and curing. Shortcomings may occur in one or several stages of this process (for instance, congested reinforcement placement, insufficient compaction, etc.), which results in defects, such as voids or honeycombing. Any decision on possible action or repair should be based on the defect's condition and the general damage level. After the formwork removal on this bridge construction project, extensive honeycombing was found on part of a concrete surface. The authors adopted the elastic wave velocity tomography method to evaluate the damage level of a newly built bridge pier with an extensive honeycomb area. Tomography results can be visualized in 3D contour plots of velocity distribution, in which regions with lower velocity correspond to regions with a defect. In this case, the initial measurement was carried out and the result showed areas with lower wave velocity in the locations corresponding to the honeycombs. Later on, the honeycombs were removed, and repair was applied by means of a new layer of concrete. After the repair, elastic wave velocity tomography was carried out again. In the resulting velocity distribution, the areas with lower velocity corresponding to the honeycombs were eliminated. Thus, the effect of repair works was confirmed. The tested

structure and results of elastic wave tomography are presented in Fig. 6.

Recently, embedded sensors have been used in concrete to evaluate the grouting efficacy and cracking repair using cement paste, cement mortar or epoxy resin grout (Zhang et al., 2022). In case the crack is in between the pulser-receiver pair, it is possible to register an increase in the amplitude after crack filling with grout (Song et al., 2008). However, the reached value remained significantly lower compared to the amplitude recorded for the intact state, indicating the dominant effect of concrete-grout interface leading to wave scattering.

### 2.1.2. One-sided evaluation

In case access to both sides is not feasible, ultrasonic inspection can be conducted by one-sided measurements and based on the surface or Rayleigh waves. These surface waves propagate only through the top surface layer at a depth roughly equal to their wavelength (Jacobs and Owino, 2000, Carino, 2003). Therefore, the waves are sensitive to the presence of a crack and its possible repair/filling up to the maximum depth of their propagation. The example of Fig. 7(a) shows the five-sensor arrangement (with separation 50 mm distance) mounted on a concrete slab with the pencil lead break excitation. This excitation is casually applied as it results in the introduction of a broad band of frequencies and is described by ASTM E976. Fig. 7(b) shows the waveforms received after wave excitation adjacent to sensor 1. It is obvious that the discontinuity of the crack (between Sensor 3 and 4) does not allow the wave energy to pass after sensor 3, with the waveforms of sensor 4 (150 mm) and sensor 5 (200 mm) showing practically no content. However, the energy at the last two sensors is substantially increased after the epoxy injection (Fig. 7(c)). The onset became clearly distinguishable while the strong Rayleigh peak appeared again allowing the measurement of longitudinal and Rayleigh wave velocities (Aggelis and Shiotani, 2007).

In an effort to quantify the filling degree, experiments and simulations were conducted on concrete beams with manufactured slots (one with depth of 19 mm and another with depth of 23 mm) and partially or fully repaired by epoxy injection (Fig. 8(a)). The amplitude of the Rayleigh wave was monotonically correlated to the filling degree. Specifically, for an empty slot (or 0% filling, Fig. 8(b)), the Rayleigh amplitude starts at approximately 35% of the maximum (corresponding to full filling). The initial layer filling of a few mm, corresponding to 15% of the entire slot depth (see Fig. 8(b)), restores the amplitude already to 60% of maximum, while at 50% of crack filling, the wave amplitude was restored to almost 70% of the maximum. The results concern a main excitation of 115 kHz, resulting in a nominal Rayleigh wavelength of approximately 25 mm, which is longer than the slot's physical size, something essential for assessing the whole depth of the discontinuity. Numerical simulations showed similar trends while the whole study demonstrated the possibility of quantifying the filling degree after epoxy injection using one-sided surface wave measurements (Aggelis et al., 2009).

Based on surface waves, "surface wave tomography" is a type of elastic wave tomography focusing on the "Rayleigh" wave that propagates along the surface, like in the above-mentioned case. The method consists of attaching an group of AE sensors to the surface of a structure in a pattern and introducing elastic waves by means of impacts of steel balls of different diameters. This allows the measurement of surface wave velocity between impact points and AE sensors. This data is then processed by the tomography algorithm, which reconstructs a tested structure's elastic wave velocity distribution. Elastic wave velocity distribution is visualized as a contour plot, where areas with low elastic wave velocity correspond to areas with defects. In the specific application, a water leak in an underground structure was monitored before, immediately after the repair and 9, 17 and 23 months later. Fig. 9(a) shows the layout of the sensors used in this inspection, as well as photographs taken during measurements. Nine receiving sensors were placed in three lines and three rows (500 × 500 mm), and impact-side sensors were placed at 16 arbitrary points. The outer receiving sensors were arranged symmetrically with respect to the defect, and the inner ones were positioned on the center line of the measurement area. This sensor arrangement made a total of 144 scan lines. The sensors used in this study were 60 kHz resonant AE sensors. The inspection showed that immediately after repair, the velocity increased, indicating the crack filling by the repair agent (Fig. 9(b)). After 9 months, there was a slight increase in velocity, which can be explained by additional hydration of the repair material due to existing moisture. After 17 and 23 months, there was a minor decrease in velocity, which can be explained by minor water leaks, observed during the visual inspection. Minor water leaks can indicate a recurrence of cracking, which can decrease the velocity. Therefore, Rayleigh elastic waves indicate the initial condition and the effectiveness of repair, while allowing monitoring at later ages.

### 2.1.3. Evaluation of crack repair using AE tomography

While in aforementioned elastic wave tomography, waves are excited at known coordinates, in "acoustic emission" (AE) tomography the velocity distribution in the region of interest is constructed by estimating the location of the source of elastic waves which are generated at unknown coordinates (Kobayashi and Shiotani, 2016). In this case, three RC slab-panels (Fig. 10 (a)) were repaired by using the epoxy injection method since web-shaped crack networks were observed after 46 years

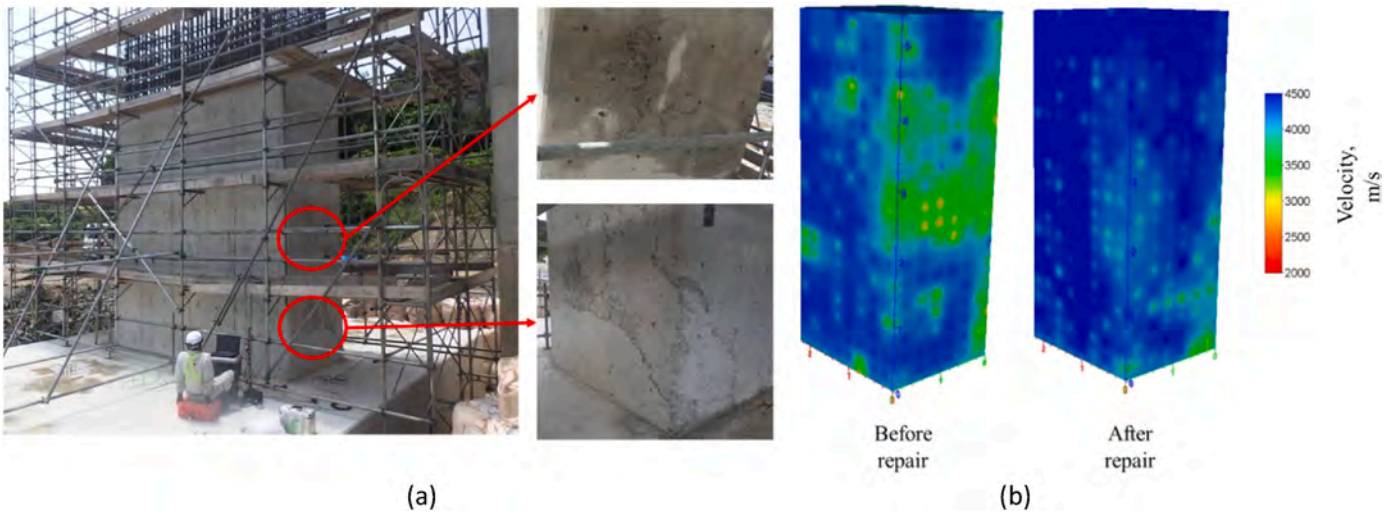


**Fig. 6.** (a) Tested bridge pier with honeycombs on the surface, and (b) results of elastic wave velocity tomography before and after repair.

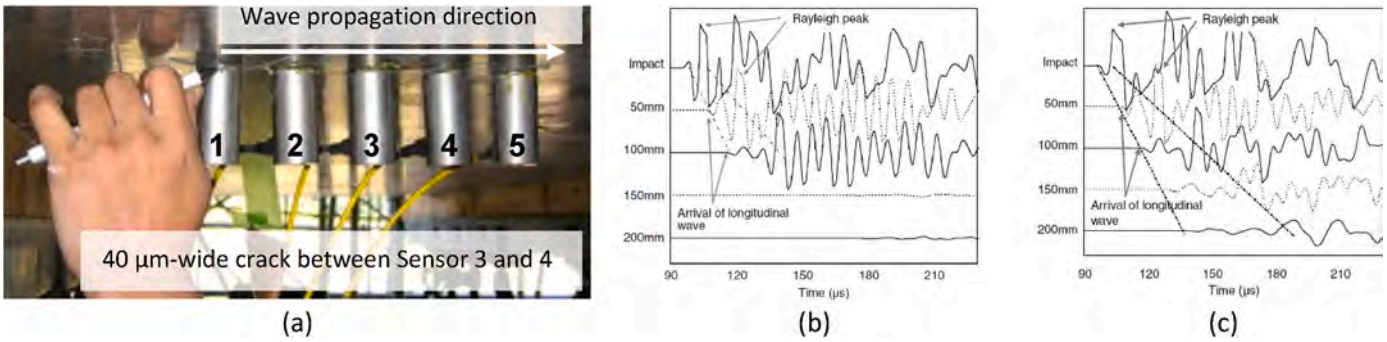


**Fig. 7.** (a) Sensor arrangement for surface wave measurement, (b) waveforms before repair, (c) waveforms after repair with epoxy injection (Aggelis and Shiotani, 2007).

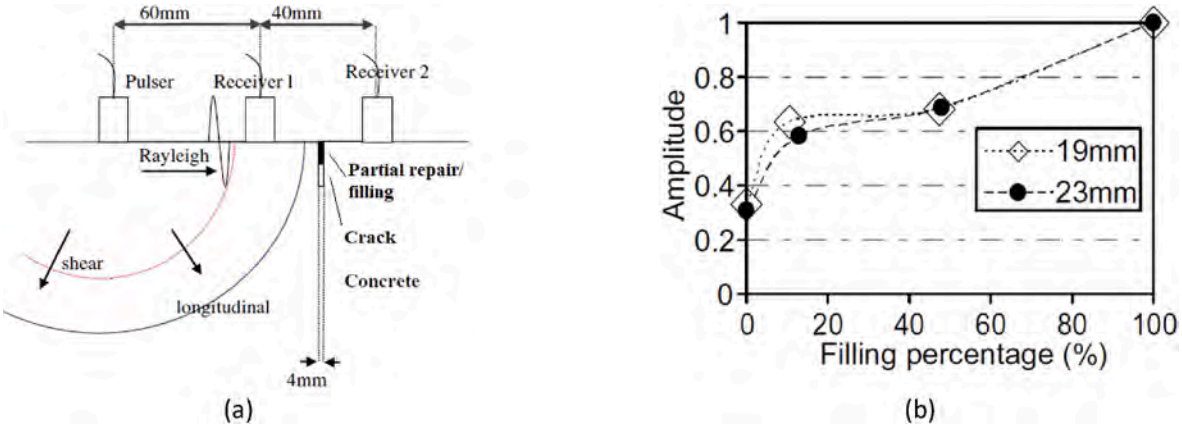


**Fig. 8.** (a) Schematic representation of testing geometry for repair assessment through Rayleigh waves, (b) Wave amplitude normalized to maximum vs. the filling percentage of cracks (Aggelis et al., 2009a).

in service. Fig. 10 (b) shows a sketch of cracks obtained through visual inspection from the bottom side of the slab. These cracks are thought to be caused primarily by the alkali-silica reaction in concrete.

Fig. 11(a) shows the model of AE tomography analysis and the positions of the sensors. The shaded part at the top of the model indicates the asphalt layer with thickness of 50 mm. As elements for AE tomography analysis, the applicable region was divided in 16 × 8, which gives a total of 128 elements. In this study, elastic waves were excited by steel-ball tapping. A steel-ball of 5 mm diameter was tapped at several locations on the asphalt surface, ensuring that the distribution of impact points was as uniform as possible at the target area. The steel-ball tapping is illustrated in Fig. 11(b) (Okude et al., 2018).

AE tomography results show that in all slab panels, the velocity after repair increased compared to before repair. Fig. 12 shows the histograms of velocities obtained in all the panels. For all slab panels, it is evident that the velocities clearly shift to higher values after repair. Due to the effectiveness of injected material in filling cracks and defects, deviations and distortions in the propagation paths of elastic waves are (partially) eliminated and the distribution of apparent velocities are increased. Low velocities, below 2500 m/s are still observed even after repair, which is reasonable because of the existence of independent voids due to air-entraining agent and limited injection in fine cracks. In addition, the propagation was partially done through the asphalt layer which exhibits a wave velocity of about 2800 m/s. This seems to contribute to the relatively low absolute values, but it is highlighted that the importance lies in the relative improvement before and after repair, while the very low values close or below 2000 m/s were totally eliminated.

#### 2.1.4. Evaluation of crack repair using elastic wave source density

The effect of repair by epoxy injection on an RC slab of a highway bridge was visualized (Takamine et al., 2018). The results before and after repair were compared to visualize the soundness based on the elastic wave source distribution by measuring the elastic waves generated by the traffic. Fig. 13 shows an overview of the measurement. The bridge of interest is a highway bridge in service, and elastic waves generated by vehicle traffic were measured for the RC slab. The target panel had cracks which were visible from the underside and was reinforced with CFRP sheets. Eighteen AE sensors were installed in a grid pattern of 3 × 6 on the underside of the deck. The sensor spacing was 780 mm in the bridge axis direction and 700 mm in the direction perpendicular to the bridge axis.

The results of the soundness evaluation before and after repair of the RC slab are shown in Fig. 14. The sound area is displayed white, and the unsound or damaged area is shown dark. The relatively damaged area has lower density of the located elastic wave sources, indicating that there are cracks or voids that hinder the propagation of elastic waves. The recovery of the soundness by repair is obvious comparing the results before and after repair (Fig. 14 a and b). In the area to the right of the slab, although the soundness (capacity to transmit AE events) has slightly improved, there are segments where the soundness remains lower. This indicates that there can be segments where resin filling is not complete and in general the method shows the ability to detect restoration after repair and to visualize repair effects in a planar (2D) manner. It is mentioned that the numbers of passing vehicles during both measurements were counted and the results of elastic wave source density are normalized by the vehicle number. Therefore, both results are compared validly even if the tested periods are different.

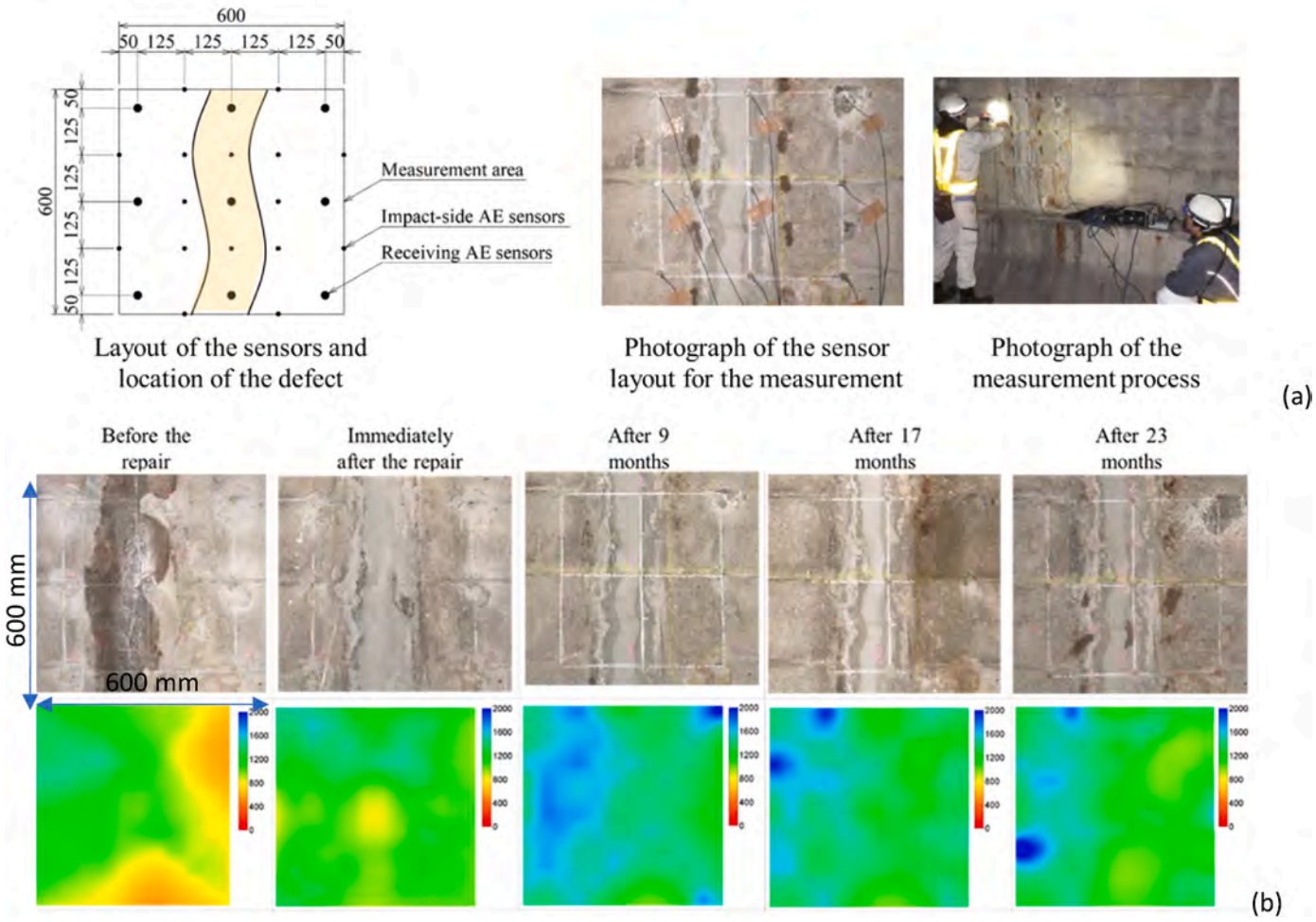


**Fig. 9.** Surface wave tomography: (a) schematic representation and photograph of the inspected area, (b) monitoring results (photographs of the surface at the corresponding times and tomograms (the colormap is in m/s, Ogura et al., 2023).

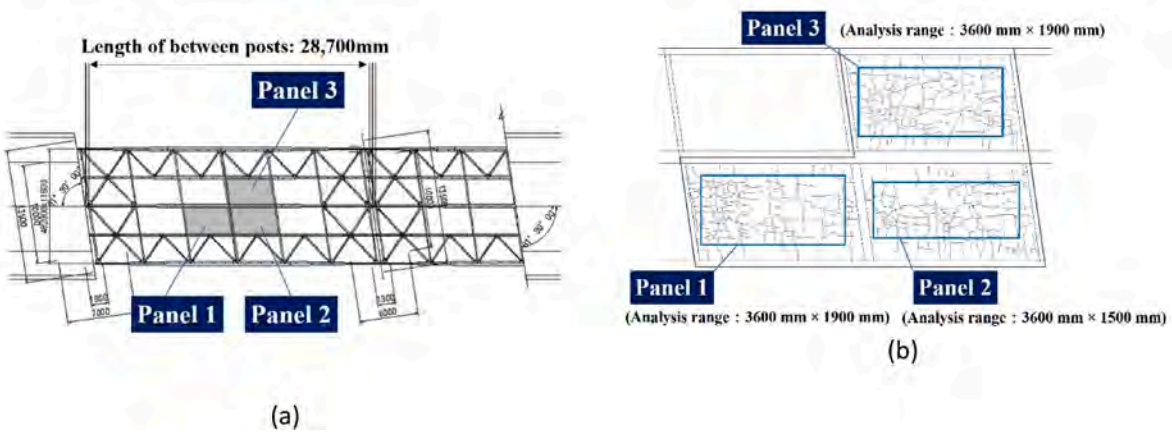


**Fig. 10.** (a) An overview of the bridge and (b) a sketch of the cracking pattern (Okude et al., 2018).

### 2.2. Repair through autogenous self-healing

Apart from manual repair, healing can take place in cementitious materials inherently due to delayed hydration and precipitation of $CaCO_3$ in the cracks. Using ultrasound, it is possible to monitor the restoration of mechanical properties due to self-healing like in manual repair. Extended wet-dry cyclic curing provides evidence of critical autogenous healing, a phenomenon directly linked to crack sealing, continuity of restoration that practically is reflected in a regain of ultrasound pulse velocity (UPV) (Aldea et al., 2000). This behavior can be enhanced by additives such as superabsorbent polymers (SAPs). In the specific case of Lefever et al. (2020), in order to create the initial crack, the mortar specimens were fractured by tensile loading after curing for 28 days. Later, they were placed in wet-dry cycles consisting of 1 h in water and 23 h in dry conditions at 20°C for another 28 days to promote healing. Changes of ultrasonic properties were monitored from the

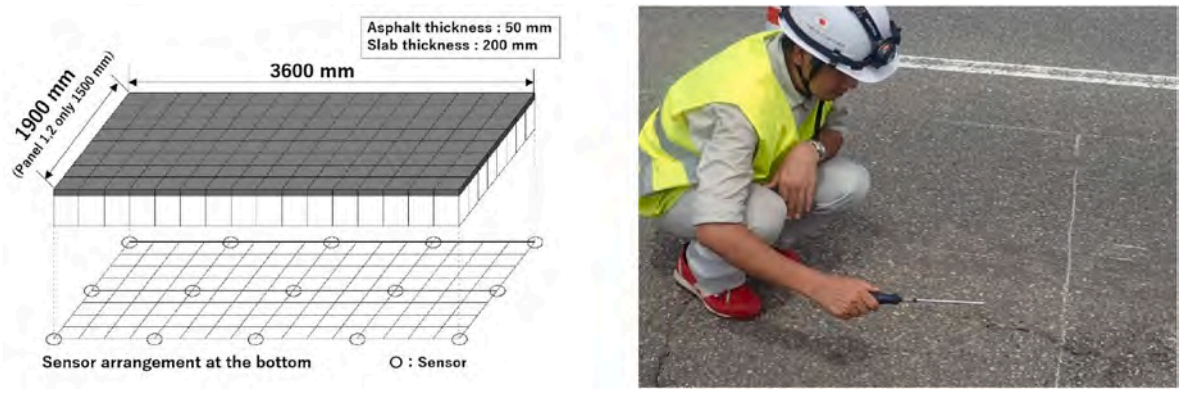


**Fig. 11.** (a) Analysis model for AE tomography, (b) steel-ball tapping (Okude et al., 2018).

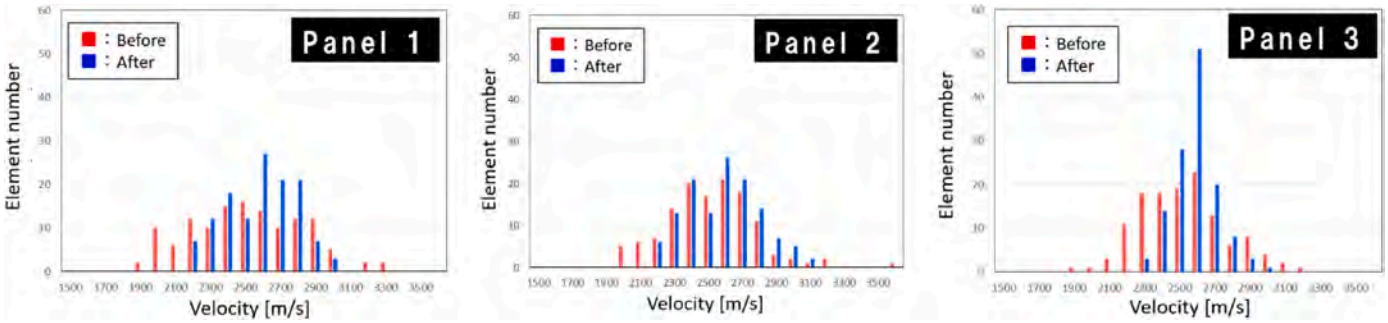


**Fig. 12.** Histograms of velocities obtained in all three elements before and after repair.


**Fig. 13.** (a) Tested highway bridge, (b) sensor arrangement for the measurement before repair.

specimen surface, mainly in the forms of wave velocity and amplitude. Two relatively broadband sensors with a peak frequency response of 450 kHz were attached on the specimen surface at both sides of the crack, see Fig. 15(a) and the excitation was conducted by pencil lead breaks. It was clear that a sharp decrease in velocity and amplitude was noticed after cracking (Fig. 15(b), see waveform 'Cracked material 0 days'). In contrast, later, with the healing progress, the wave amplitude was restored towards the original level.

Since self-healing depends strongly on the conditions and, specifically, the availability of water, it is expected that it is more effective on the surface of the specimens rather than deeper in the crack. This can be checked using the above-mentioned surface wave setup. The reason is that, as aforementioned, surface or Rayleigh waves penetrate at a depth roughly equal to their wavelength. Therefore, pulses of short wavelengths (or high frequencies) are more indicative of shallow layers. In contrast, long wavelengths or low frequencies also collect information from deeper layers. Fig. 15(c) shows the attenuation curve for an indicative mortar mix (with cement type CEM I and nanosilica particles before cracking, after cracking and 14 days after wet-dry cycles (Lefever et al., 2020). The initial (uncracked) curve is at relatively low values and shows an increasing trend since the higher frequencies are normally more effectively damped and scattered by the inherent microstructure. As expected, the through-the-thickness crack sharply increases the level of the apparent attenuation by about 5 times (i.e. from the level of about 0.2 dB/mm to almost 1 dB/mm, 'cracked' curve). The wet-dry cycles until 14 days have a certain decreasing effect on the attenuation. Since healing products are precipitated in the crack, wave transmission is partially restored and the attenuation curve at '14 days' is lower. Furthermore, it is indicative that higher frequencies show a stronger decrease after healing, than lower ones. Indicatively, attenuation drops by approximately 0.3–0.4 dB/mm at the zones around 800 kHz, while it drops by about 0.1 dB/mm or less around 200 kHz. This confirms that

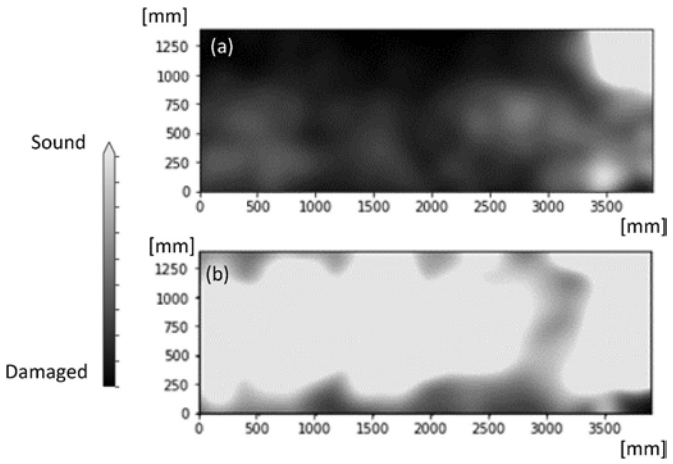


**Fig. 14.** Results of elastic wave analysis (a) before repair and (b) after repair.

the deposition of healing products is more effective in a layer of 3 mm (Rayleigh wavelength of 800 kHz), while wavelengths propagating as deep as 10–12 mm (200 kHz) show less restoration. It is mentioned that at the sound and fully healed stage, the attenuation can be more safely attributed to Rayleigh waves, while for the cracked stage, due to the severe discontinuity, Rayleigh waves are not easily discernible. This apparent attenuation, therefore, is a measure of the whole transmitted energy of the wave modes near the surface.

The restoration degree of the pulse velocity or attenuation gives a measure to quantify the self-healing. However, this applies to the wave parameters and is not directly translated into mechanical properties restoration. In an effort to better relate the restoration of wave parameters (amplitude, wave velocity) to the stiffness of the healing products, a numerical study was recently reported (Fig. 16(a) (Lefever et al., 2022a)). There, the equivalent stiffness of the healing material was varied to check its effect on the macroscopically measured pulse velocity and attenuation. At zero stiffness, the Rayleigh wave is not transmitted through the crack and is completely reflected as shown in Fig. 16(a). In the case of a material with considerable stiffness inside the crack, the Rayleigh wave is partially transmitted (Fig. 16(b)). It was found that the early healing (i.e. increase of the Young's modulus of the healing product from 0 to 1 GPa) is already responsible for approximately 60% of the restoration of the wave velocity and amplitude while further hardening of the healing layer, has a smaller effect, see Fig. 16(c). Therefore, surface ultrasound is sensitive to healing and especially the initial crucial stage of healing product formation, which makes the difference between the discontinuity (empty crack) and an elastic medium that can support elastic waves, showing a minimum of mechanical properties. Considering that the experimental restoration of the wave velocity and amplitude was also at approximately 60% (Lefever et al., 2022a), it was concluded that the healing products were of the order of 1 GPa after 28 days of healing.

The example mentioned above was taken for one-sided surface wave

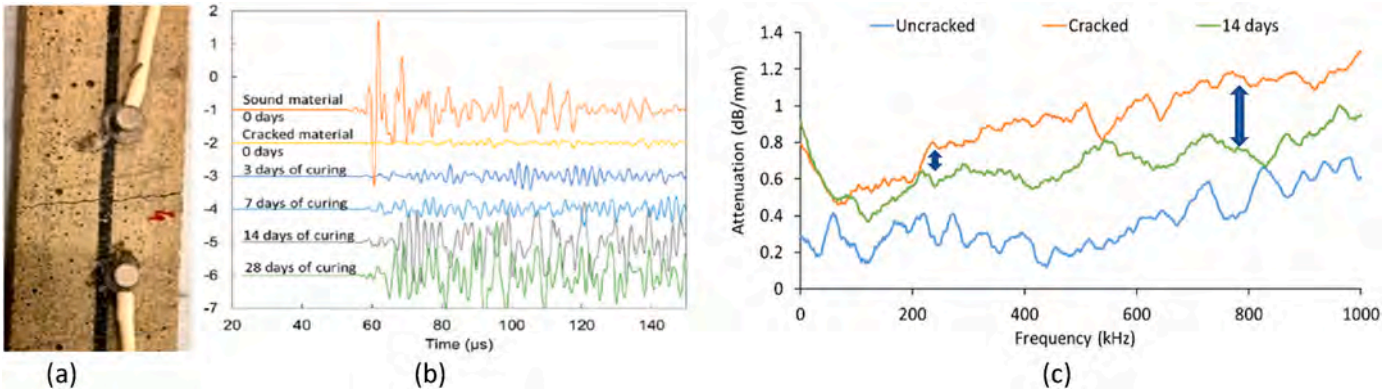


**Fig. 15.** (a) Pico sensors placed at both sides of the crack in a mortar specimen, (b) waveforms after the crack for different conditions of the cracking and healing ages, (c) surface wave attenuation vs. frequency curves for intact, cracked and partially healed mortar with nanosilica (Lefever et al., 2020).

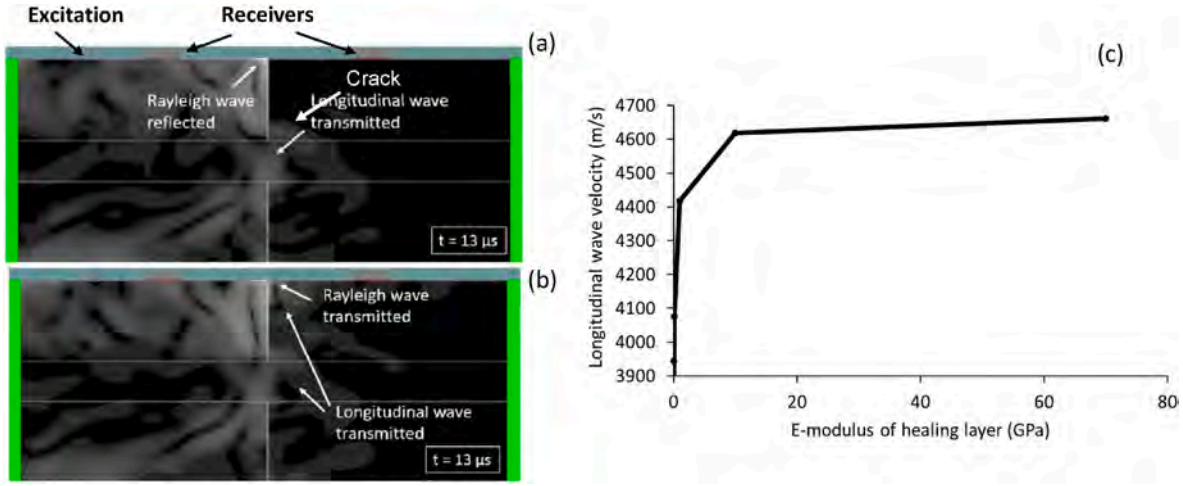


**Fig. 16.** Simulated wave displacement field in mortar (a) in the presence of crack (b) with healing agent in the crack, (c) simulation of wave velocity dependence on E-modulus of healing material (Lefever et al., 2022a).

propagation. In case the through-thickness application is possible, ultrasonic mapping can be conducted through longitudinal waves with pulser and receiver in a face-to-face configuration, as shown in Fig. 17 (a). In this example (Lefever et al., 2022b), cracks were created by the Brazilian test (Fig. 17(b)), and the specimens were similarly cured in wet-dry cycles as mentioned above. Some specimens included SAPs aiming at promoting healing. Based on the pulser-receiver transit time, the UPV for all direct horizontal paths is calculated and presented for a typical case at different ages: sound condition (Fig. 17(c)), cracked condition (Fig. 17(d)), and after 28 days healing (Fig. 17(e)).

Cracking has a direct effect in reducing the overall velocity from the level of 4000 m/s to 2000 m/s. Later, propagation was restored close to 70% of the original level (Fig. 17(e)), with average velocity reaching approximately 3400 m/s. Ultrasonic maps of more ages can be seen in the original publication (Lefever et al., 2022b), indicating not only a general level of restoration but also the distribution or level of uniformity of healing, which is challenging to evaluate with other assessment techniques. Attenuation results were on the same line, while microscopic measurements of the crack width revealed similar trends: the crack width decreased, but was not completely eliminated. The above shows that wave propagation is advantageous for monitoring cracking as well as repair through healing, while non-contact sensors are recently employed to avoid coupling variability (Lefever et al., 2024).

In another recent study, through transmission during autogenous healing was utilized. Kaur et al. (2019, 2020) applied the short-time Fourier transform (STFT) to analyze the frequency content of the signal transmitted as bio-cementation takes place. Specifically, concrete samples were cracked (opening up to 0.7 mm), and the crack was then filled with bacterial-cementitious fluid. A Fourier Transformation was performed on received signals emitted through the cracked zone and generated with 200 kHz central frequency. A time-frequency window that includes the signal intensity variations as healing evolved was isolated. An exponential signal intensity increase was reported while the bacteria sealed the crack, as demonstrated by simultaneous hydraulic flow tests that tracked the crack's water tightness.

An earlier study based on resonance frequency on concrete specimens is also worth mentioning (Jacobsen et al., 1995). After exposure to freeze-thaw, the dynamic modulus dropped to even 51% of the original for ordinary Portland cement (OPC) and 23% for OPC with silica fume. However, after storage in water for 3 months, the dynamic modulus, as measured by resonance frequency, increased to 97% and 72%, respectively. The specific test is not detailed in the document, while the specimens were cubes of 100 mm side. The compressive strength did not restore to similarly high values after healing (Jacobsen et al., 1995). Coming from the same group, another study utilized UPV on concrete cylinders after three months of rapid freeze-thaw damage (freezing in air, thawing in water) and self-healing in lime-saturated water. It was seen that after the initial recovery due to damage, a strong recovery in UPV was noticed between 50% and 100%. At the same time, it was concluded that the stronger the initial damage, the weaker the final recovery. In this case, the compressive strength showed a much lower recovery rate as well (Jacobsen et al., 1996).

In Sahmaran et al. (2008), concrete specimens with and without fly ash inclusion were damaged by loading at different levels of their expected strength (70% and 90%) to create cracking before being subjected to healing cycles in lime-saturated water. UPV measurements showed a clear decrease after cracking of the order of 5–10%, while healing for a duration up to 30 days restored UPV nearly to 100% for both loading levels. Compressive strength decreased by 20–30% while after 30 days of healing it was approximately 10% lower than the pristine specimens. A similar study (Zhong and Yao, 2008), based on 30–60 days of healing in a standard curing room after damage under compression, showed a substantial recovery of UPV for normal and high-strength concrete cubes of 100 mm side. The authors concluded that there is a "damage degree threshold" above which the healing degree weakens with increasing damage.

### 2.3. Repair through autonomous self-healing

Another self-healing approach that has gained the attention of the scientific committee over the last decade is the autonomous self-healing, which involves the use of healing agent carriers that are encapsulated in concrete during casting and would break under mechanical stresses as a crack propagates through the capsule to cause release of sealant that fills the crack. Elastic wave inspection plays a key role in the assessment of concrete repair after the healing activation. Specifically, Van Tittelboom et al. (2012) proposed the embedment of glass capsules in concrete that would carry a polymeric agent that, upon breakage, would fill up the crack. The UPV appeared to be a direct and reliable tool for the repair efficacy assessment (Muhammad et al., 2016). As pointed out in Fig. 18, the UPV, as measured in transmission mode through concrete beams cracked under three-point bending with crack openings up to 0.3 mm, is significantly recovered after the healing agent release and curing of the agent up to 24 h in ambient conditions (Vangansbeke et al., 2023).

In parallel, the research focused on replacing the prototype glass

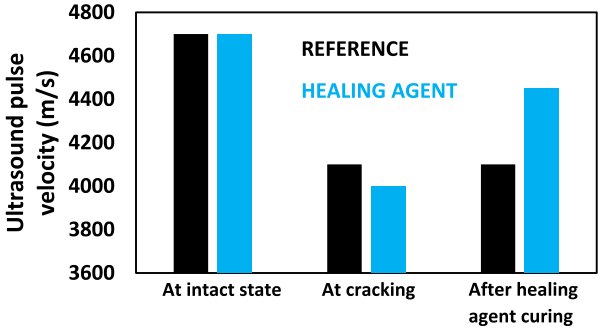


**Fig. 18.** Ultrasonic pulse velocity for reference mortar and mortar with encapsulated healing agent (Vangansbeke et al., 2023).

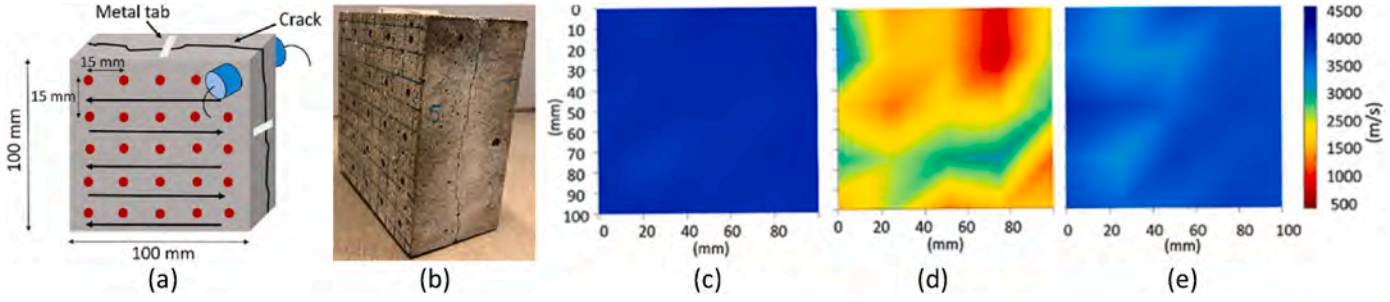


**Fig. 17.** (a) Schematic representation of the ultrasonic face-to-face measurements for self-healing evaluation, (b) photograph of the specimen with the initial crack, ultrasonic velocity visualization of a cross-section at different stages (c) sound, (d) cracked, (e) after 28 days of healing (Lefever et al., 2022b).

tubes with other carriers that are more durable and chemically compatible to concrete materials. AE monitoring during loading could detect the glass tubes brittle fracture since AE hits with higher energy compared to AE hits originating from concrete fracture were captured. This way, the healing activation moment could be identified, but also the cracking area where agent was locally released could be localized (Tsangouri et al., 2013). Similarly, to the aforementioned case of grouting, embedded sensors have been used to evaluate the repair process on concrete beams loaded under three-point bending after tubes fracturing and healing agent release into cracks. Apart from the wave velocity, other parameters can be utilized like the Root Mean Square Deviation (RMSD) value between two signals captured at intact state and at different stages over testing: at cracking or after healing or re-cracking phases. This so-called "damage index" showed a limited recovery after healing activation exhibiting some potential for evaluation of repair (Tsangouri et al., 2015). In an advancement in the field, the second generation of autonomous healing concerns the design of vascular networks for optimized and repeatable healing agent distribution into cracks in larger bulk concrete elements (Tsangouri et al., 2022). Once again, UPV provides a direct proof of crack healing as demonstrated in Fig. 19(a), where the UPV recovery after healing is evident compared to the cracked stage. Remarkably, the linear networks tested in this beam configuration loaded under four-point bending achieve repair and crack sealing with polymeric agent in a large range of crack sizes, from 100 to 600 μm. An ultrasonic map is demonstrated in Fig. 19(b), where light yellow and green areas mark the zones where crack filling was reached after the healing agent distribution through the cracks. The healed zones were limited to several centimeters depth and were sporadically distributed in concrete. This result confirms that more effort should be put in improving the agent adhesion and sealing capacity.

On a larger scale, assessment of self-healing was conducted for a concrete slab. Healing was supplied by a smart capsules network (Fig. 20 (a)). After creating cracks using four-point bending loading, the specimen was allowed to heal by supplying healing agent through the network. AE tomography was applied before and after healing and the results are shown in Fig. 20 (b) and 20(c) respectively. At the end of loading, certain areas close to the middle of the slab exhibited a low velocity of even 2000 m/s which is indicated in red. After eventual healing, the tomogram revealed elevation of the velocity in average, while the specific low-velocity zones were eliminated. Cores were also extracted at different areas with high velocity restoration and confirmed the tomography result by the visual observation of the healing agent, as well as UPV measurements at different heights. A limit in the crack opening susceptible to healing with this system was suggested, since cracks with openings larger than 0.5 mm did not show any recovery, while cracks with openings smaller than 0.5 mm in the capsule network, exhibited eventual rise of velocity above 3500 m/s (Tsangouri et al., 2019).

### 2.4. Repair by thermally-activated polymer-fillers

Continuing in cases related to self-healing, Textile Reinforced Cement (TRC) plates with and without healing polymer powder were first thermally cracked and later mechanically loaded in bending (Fig. 21(a)). Exposure to high temperature led to extensive cracking, one of the basic damage mechanisms for this material, while the others are debonding between successive plies and fiber pull-out. When cracking is already saturated (in the thermally cracked specimens), the debonding phase is accelerated, resulting in a much different AE behavior. This is due to the different micro-displacement of the crack sides. In case of debonding, shear stresses emit most of the energy in the slower shear wave mode than the longitudinal waves that are mostly emitted by the tensile cracking. Therefore, for debonding associated signals most of the energy arrives later in the waveform, increasing the rise time (RT, Fig. 21(b)), as well as the overall signal duration, while it inversely decreases the frequency content. However, in the specimens with healing polymer (El Kadi et al., 2017), an almost-complete restoration of the AE properties towards the reference specimens was observed. Indicatively, the intact specimens exhibited RA-value (calculated as rise time, RT, over Amplitude, A, see Fig. 21(b)) of less than 600 μs/V, while that of the thermally cracked specimen achieved almost 1500 μs/V. The healed specimen exhibited less than 800 μs/V in RA-value, much closer to the original value. Similar was the restoration of the frequency content, indicating that cracking was again the dominant mechanism and that the behavior of the healed specimens was closer to the intact ones rather than the thermally damaged ones. The reason was that although the high temperatures produced distributed cracking in the matrix, at the same time, melted the polymer powder directly filling or repairing these cracks. Wave transmission was also indicative since thermal cracking increased the attenuation coefficient from 0.084 dB/mm to 0.137 dB/mm, while the healed material was restored to the levels of intact (Fig. 21(c)).

### 2.5. External repair patches and retrofit of concrete

Although the application of Fiber reinforced polymer (FRP) or TRC for concrete members has offered many advantages, there have been issues and concerns associated with their long-term performance including their debonding from a concrete surface or within a concrete element. Accordingly, despite their durability, concrete elements strengthened with FRP materials need to be inspected periodically to detect potential issues and hence prevent any premature failures. In Feng et al. (2018), the repair of cracks by external patches is tracked in a numerical work where cracks are filled by mortar and then covered by carbon fiber reinforced polymer (CFRP) sheets. The emission of a pulse is simulated and the received signals are compared in the time-domain and by using the wavelet packet-based energy. Both the signal amplitude and energy recover after the cement grouting of the cracks.

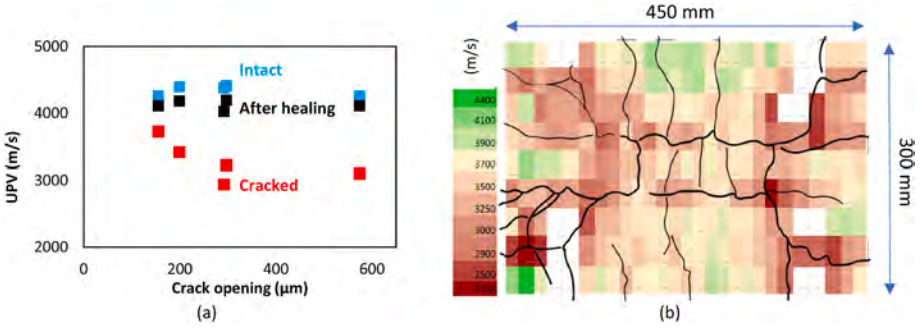


**Fig. 19.** (a) UPV measured through transmission in several concrete beams loaded in four-point bending and healed by agent distributed through a linear tubes network, (b) Ultrasound mapping of a concrete slab healed by agent distributed through vascular networks of 3D printed polymeric tubes (Tsangouri et al., 2022). The thickness of the slab is 55 mm and it is reinforced by four Φ8 ribbed steel rebars.

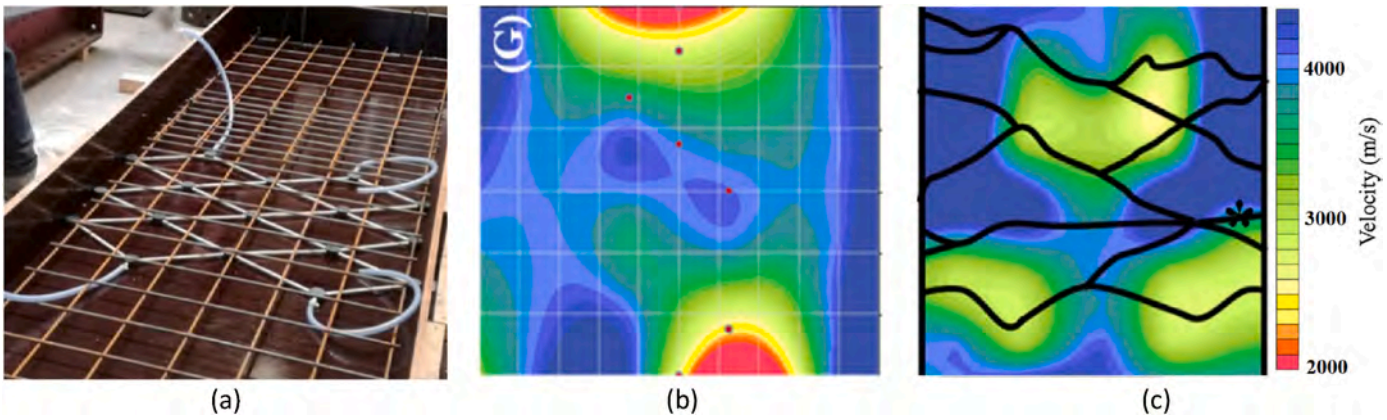


**Fig. 20.** (a) Vascular network of capsules and steel mesh before casting of the concrete slab, (b) velocity tomogram after loading, (c) velocity tomogram after healing (Tsangouri et al., 2019). The solid dark lines indicate the surface pattern of cracks, that partially reflect the position of the healing system.

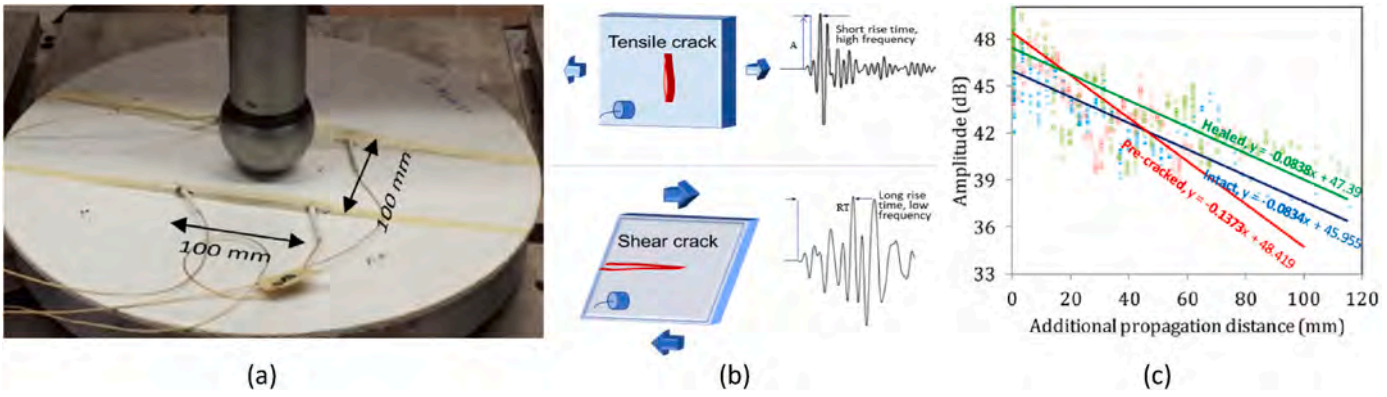


**Fig. 21.** (a) Circular TRC plate under point loading with four AE "pico" sensors, (b) different fracture modes with corresponding AE waveforms (cracking and debonding) as measured by piezoelectric sensors attached on the surface, (c) amplitude vs. distance of AE signals for different material conditions (El Kadi et al., 2017).

However, this phenomenon is masked by highly attenuated wave energy in the case that a repair patch is added due to the additional introduced interfaces. The numerical simulation of Rayleigh wave propagation through the FRP patch and damaged concrete interface has also proven to track scattering attributed to interfacial debonding phenomena (Mohseni and Ng, 2019). As validated by analytical solutions and experimental tests using laser Doppler vibrometer, the wave scattering increases through layers and interfaces after repair. It appears that the forward scattering component of the Rayleigh wave is more sensitive to the size of repair patch debonding demonstrating larger magnitudes and less complex directivity patterns. As expected, the interface morphology and texture control the adhesion between the damaged concrete and repair layer, and eventually determine the long-term performance of this repair intervention. The through the thickness inspection by elastic waves appears challenging, however, it is a unique solution for the assessment of interfacial bonding. In a previous study (Santos et al., 2010), the reflections detected from the pulse propagating through a repaired concrete were linked to the interface properties. A Finite Difference Method applied with the use of Wave 2000 plus software shows that in the presence of a rough interface, the pulse amplitude drops and greater wave dispersion is exhibited. The work is based on the analysis of Kwasniewski and Garbacz (2008) that studied the impact-echo response on parametric variations of the repair concrete interface quality. Scattering and pulse distortion may mask the effect of bonding. However, considering that the current rehabilitation interventions are designed based on cement mortars, without adding large aggregates, the method's precision is acceptable.

AE in combination with DIC produced valuable results in case of retrofitting of concrete beams with external patches either of TRC or CFRP. The beams were tested in four-point bending along with 8 AE sensors. It was noticed that for the externally repaired beams there was a clear delay in registering AE events, which is indicative of the reinforcement against cracking. Indicatively, the first AE events were localized at 16 kN for the reference beam, while for the TRC retrofitted beam at almost 41 kN, showing the beneficial effect of the external reinforcement (Aggelis et al., 2013).

In addition, the AE parameters showed distinct differences, especially at the transient load drops. For the reference beams, parameters did not show big changes implying that the fracture mechanism was essentially the same throughout loading (i.e. matrix cracking), while for the externally retrofitted beams, during the transient load drops the RT and RA values were approximately double, indicating that at that moment, debonding of the patches was happening. This was confirmed by DIC showing a sudden release of strain on the debonded patch areas, allowing the determination of the exact area where the repair/retrofitting layer was debonded (Fig. 22, Aggelis et al., 2016).

In the next example, embedded piezoelectric sensors, called smart aggregates (SAs) were used to monitor the connectivity of a concrete overlay in a repair project for tunnel (Cheng et al., 2022). Due to extensive corrosion of the reinforcement on the tunnel's bottom floor, renovations began in 2018. The old concrete cover was removed, the reinforcement was cleaned, and a new concrete layer was applied. To monitor the quality of the repaired layer and detect any potential delamination between the existing and newly-cast concrete, a total of six SAs (SA1 to SA6) were embedded in the repaired floor. Four were placed in pre-drilled holes in the old concrete, while two were placed in the


**Fig. 22.** Quantification of the debonding area of repairing TRC patch from concrete substrate by DIC strain difference before and after two load drops (Aggelis et al., 2016).

newly-cast concrete. The sensors formed ray paths across the old and new concrete and their interfaces. Potential changes in wave velocity between the ray paths across the interfaces would indicate potential delamination. Over a two-year period, measurements were taken, and the comparison of wave velocities in different ray paths did not indicate any delamination in the newly applied concrete cover (Fig. 23). The method is demostrated to be effective for long term monitoring of repair patches.

### 2.6. Repair long-term performance when exposed to weathering

Apart from the evaluation of the repair work itself, the durability of repair patch solutions for concrete structures can be evaluated as well based on elastic-wave monitoring. In recent works, accelerated weathering tests were performed on concrete repaired by cement and polymer composites. The micro-cracks developed on the cement and polymer-modified cementitious repair layer after exposure to freeze-thaw are correlated to the loss of dynamic elastic modulus ($E_{dyn}$) as tracked by the 1st-mode resonant frequency variations (Wang and Gupta, 2021). The tracking of $E_{dyn}$ by non-destructive inspection provides an indirect and accurate estimation of the repair damage state and can pinpoint premature debonding compared to conventional pull-off and tensile splitting tests. The weathering exposure of CFRP external repair patches for concrete is associated with premature interfacial debonding, a result that is also validated by the surface acoustic wave inspection in Mahmoud et al. (2010). Narrow-band transducers with a 110 kHz central frequency were mounted on the repair patch surface to generate stress waves that were received by identical probes, to obtain the energy and frequency related parameters. The variables shifts are tracked under accelerated aging conditions for 12 weeks showing considerable changes and are linked to internal debonding and mortar degradation as verified by the drop of fracture energy in the test campaign that followed.

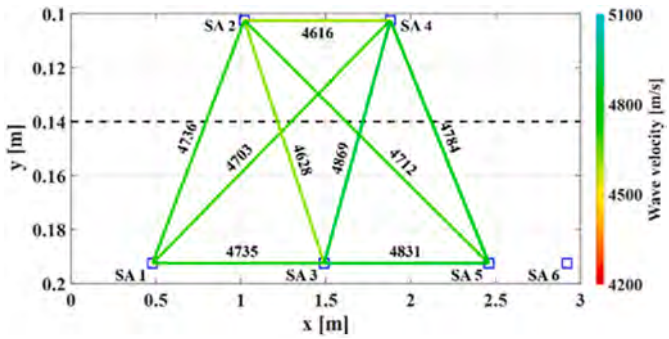


**Fig. 23.** Wave velocity in each ray path on the 757th day (Cheng et al., 2022).

## 3. Beyond concrete

### 3.1. Marble

Work is scarce in repair evaluation of structures made of marble, with only one study identified in estimation of repair. This was conducted with epoxy agent directly applied on the fracture surface after three-point bending. Although ultrasound shows sensitivity to the damage condition of marble (see for example Papasergio et al., 2023), UPV was not very sensitive to the adhesion conditions between epoxy and the fractured marble surface. On the other hand the change in AE behavior was much more indicative. Practically, the healthy specimens exhibited three main stages of AE behavior during loading; initial stable increase of AE, then a period of silence and finally another increase of AE acquisition ending with a sharp spike during the final collapse of the brittle material. After repair, most of the specimens showed the same AE behavior (high initial rate-plateau-high final rate) while in others, distinct stages could not be defined. For the first group of repaired specimens the restoration degree, measured by the ratio of the maximum load at reloading over the maximum load at initial loading, was much higher, showing that when adhesion repair is adequate, the AE recording at early stages can give a good estimate of the restoration (Tsangouri et al., 2016).

### 3.2. Masonry retrofit

Static and seismic safety of historic buildings need to be improved through techniques that often must be calibrated ad hoc for the individual case study, in order to achieve a balance between safety and the preservation of the original historical-architectural features. The evaluation of the effectiveness of the strengthening and seismic improvement works of the historic masonry structures is a very complex operation due to the great variety of masonry textures and different repair techniques (Grazzini and Lacidogna, 2021). Non-invasive diagnostic techniques, in addition to being used in situ to deepen the knowledge of the qualitative characteristics of masonry, can also be used for a preliminary evaluation for the choice of the most suitable material and strengthening techniques, as well as being able to validate the repair work after its execution. Faced with many technologies of intervention, the choice of the repair material, in fact, is often decisive for the durability and effectiveness of the same, in particular in the field of cultural heritage (Bocca et al., 2014).

### 3.3. Repair on multiple leaf stone masonry

In the case of masonry, mechanical testing combined with AE measurements aims to check if repair is effective, as well as if repair with injections is enough to bind the wall layers. If not, alternatively cross bars injection efficacy for repair should be assessed by AE as well

(Anzani et al., 2008). The test specimens (see Fig. 24(a)) were instrumented with 6 AE sensors, which allowed to localize the points of initiation of the cracks and interpret their trend during loading. After repair, masonry test specimens reinforced by steel rods, mortar injection, or a combination of both (Fig. 24(b)) were monitored with AE throughout the loading test. Samples were loaded under stress control, imposing constant speed of displacement. Cumulative AE counts increase slowly in the first load phase, after which they increase proportionally to the load, reaching a peak close to the test failure load (Fig. 25 (a)). The function representing the count rate (AE counts number per minute) reaches its maximum value in the ascending branch of the load-displacement curves and is then reduced to zero in the proximity of the final load. It is, therefore, possible to identify two phases during testing: a first phase during which the largest cracks are formed and the material reaches a critical damage condition (Phase 1), and a second phase during which the material tends to exhaust its load capacity (Phase 2). For the repaired specimen with mortar injection and steel rods, the cumulative AE activity was notably lower (less than one third of the reference) (Fig. 25(b)).

In the AE field, the "b-value" is calculated by analogy with seismic phenomena. It stands for the proportion of low-intensity events over the high energy events and is calculated as the slope of the inverse cumulative amplitude distribution (Fig. 26). Low absolute b-values indicate the progress of the fracture towards larger scale events that occur at the limit of the load-bearing capacity of the component (Carpinteri et al., 2009, 2011). This parameter changes systematically at different stages in the course of the damage process and, therefore, can be used to estimate damage evolution modalities. By applying these concepts to different specimens, unreinforced (PS6) and reinforced with mortar injection and steel rods (PN4), it can be seen that the former exhausted its bearing capacity during the load test, with the formation of cracks of a size comparable to that of the specimen, forming along the interface between the filler and the outer wall (b-value $\cong$ 1), and the latter, characterized by a widespread cracking pattern, still has a reserve of strength before reaching the final collapse (b-value $\cong$ 1.7). The determination of the "b-values" for the two specimens is shown in Fig. 26, which is based on calculating the gradient of linear regressions obtained from Log N versus m plots. In seismicity N is the cumulative number of earthquakes with magnitude $\geq$ m in a given area and a specific time-space. While in AE analysis N is the cumulative number of AE signals whose magnitude is calculated as m $\propto$ Log 10 Amax, Amax being the maximum amplitude of the signals (Anzani et al., 2008).

### 3.4. Debonding of composite masonry strengthening systems

In terms of quality control and evaluating the effectiveness of repair and strengthening interventions, it is also important to be able to detect possible failure of the strengthening techniques (Saidi et al., 2022). Therefore, the AE technique was used to investigate damage in composite masonry strengthening systems with a polymer- or mortar-based matrix (Ghiassi et al., 2014; Verstrynge et al., 2016). More specifically, clay bricks were strengthened with Glass Fibre Reinforced Polymer (GFRP) and with Steel Reinforced Grout (SRG) and were tested during single-lap shear bond tests (Fig. 27). It was observed, based on localized AE events, that delamination started at the loaded end and moved downward during testing, according to the expected movement of the debonded area. A clear distinction based on the AE energy was found between specimens showing different failure modes, i.e. GFRP cohesive or adhesive failure (Fig. 28(a)) and SRG brick/mortar detachment or fibres slipping (Fig. 28(b)). It can be concluded from these tests that the AE technique can characterize the failure mode of GFRP- and SRG-strengthening debonding.

In a similar study, the progressive failure under shear bond testing of carbon TRC retrofitting layer mounted on brick masonry is tracked with AE source localization method in correlation to DIC as illustrated in Fig. 29 (Linn et al., 2022). The vertical Eyy strains were mapped at different loading stages as multiple cracks progressively form along the TRC retrofitting patch, while, below, the AE events distribution along the vertical axis are plotted as well at the same loading stages. For both the visual DIC analysis and the AE events localization tracking method, the cracks (associated with AE events) initiated at the top side of the patch and propagated towards the bottom of the TRC patch. It was evident that AE can accurately monitor the damage evolution and precisely pinpoint the damage front at any moment during a single-lap shear test.

Moreover, the AE technique was applied to investigate the thermal incompatibility between epoxy-bonded FRP and masonry compared to a mortar-based (SRG) application during temperature cycles. The specimens were exposed to 180 temperature cycles in a climate chamber. In each cycle, the temperature was kept constant at 10 °C for 2 h. The temperature was then increased towards 50 °C for 1 h, followed by 2 h at a constant temperature of 50 °C. Afterwards, the temperature was decreased again towards 10 °C for 1 h, resulting in cycles with a duration of 6 h. Fewer and more randomly emitted AE events were observed in the case of SRG-strengthened specimens. In contrast, each temperature decrease for FRP-strengthened bricks led to higher AE energy release. This can be interpreted as an indication of the different damage sources. In case of SRG-strengthened specimens, the AE events reasonably originated from further curing or mortar micro-cracking. In the case of the FRP-strengthened bricks, the decrease in AE energy during temperature changes is due to the thermal incompatibility between the epoxy glue and the brick, as the thermal expansion coefficient of epoxy can be up to

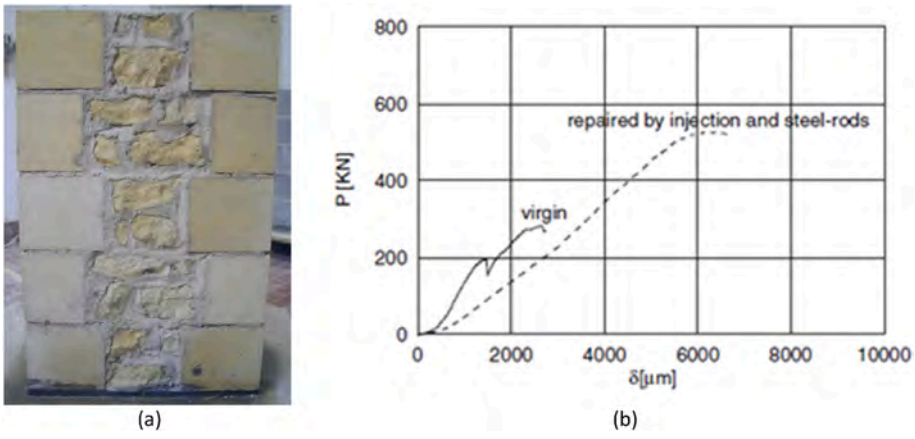


**Fig. 24.** (a) Typical geometry of the tested walls, (b) Load-displacement curves of masonry wall component (PN4) in Noto stone (reference and reinforced by mortar injections and steel rods) (Anzani et al., 2008).

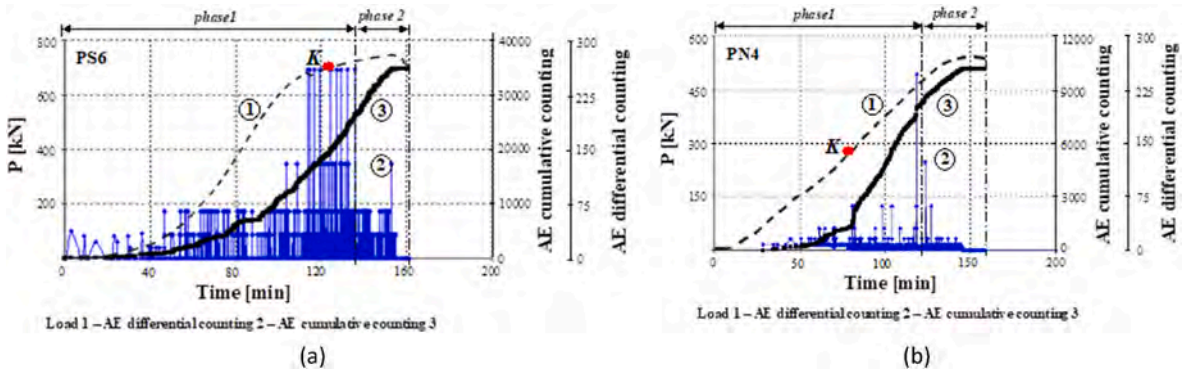


**Fig. 25.** Load/AE activity-time curves for walls PS6 (reference) and PN4 (repaired) (Anzani et al., 2008).

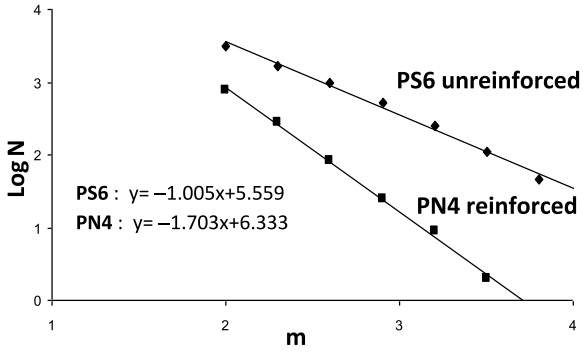


**Fig. 26.** Determination of "b-value" at the end of the loading test on the two specimens (Anzani et al., 2008).

10 times larger than that of brick. This difference may lead to damage propagation at the brick-FRP interface during thermal cycles. It should be noted that relative shifts of the AE parameters are more important than absolute values as these absolute AE parameters depend strongly on the sensor type, propagation distance and material properties.

Besides the AE technique, infrared thermography can be applied to detect debonding. This was done in Ghiassi et al. (2013) on similar test specimens aged the same way as described before. With infrared thermography, the surfaces of the specimens are exposed to thermal energy for a short period, while not damaging the composite system, and the changes in the surface temperature of the heated material are recorded as sequential thermal images or videos during the cooling process. Two lamps with a maximum capacity of 2000 W were used as heating sources. The lamps were placed at a 500 mm distance from the surface of the specimens. The existence of discontinuities, such as interfacial defects or delaminations, affects the thermal properties. The temperature decay in degraded areas is altered, which can be identified as hot spots in the thermal images, as exemplified in Fig. 30. This test provides a picture of the potential detachments. However, high thermal conductivity (carbon or steel fibres) or high matrix thicknesses could limit the detectability of the test.

### 3.5. Debonding process in repair plasters

In order to examine the bonding conditions and the general mechanical behavior in coupled materials consisting of stone and repair plaster, "triplet" specimens were subjected to compression with the concurrent acquisition of AE (Fig. 31(a and b)). This way, the fracture mode at the interface between the two materials can be examined (Grazzini et al., 2020). The test is helpful in assessing the compatibility of new repair mortars against the historic masonry support, to whose interface often stresses arise due to the excessive rigidity of the repair mortars when they are stressed by thermal or mechanical cycles.

As aforementioned and shown in Fig. 21(b), the shape of the AE waveforms is typical of the fracture mode, with shear events, characterized by longer rise times, and lower frequencies than the waveforms related to tensile mode fracture. Through the analysis, it was possible to identify a first phase of the test in which a fracture of mode I for traction prevails (AF values up to 300 kHz), followed by a shift to mode II for shear load during the delamination process (events with frequency of approximately 100 kHz). This study is more related to the evaluation of compatibility (similarity in mechanical characteristics) and durability over time when subjected to fatigue cycles and is not directly connected to the successful application of the repair. However, it is included in this report to show how relevant the interface bond compatibility is for a broader interpretation of repair on masonry and for assessing of the

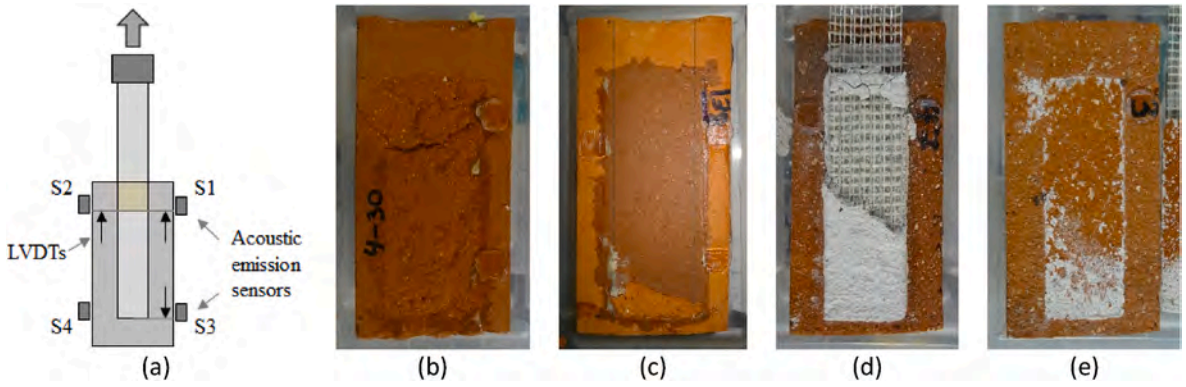


**Fig. 27.** (a) Setup of shear bond test with AE monitoring, pictures of observed failure modes: (b) FRP cohesive failure, (c) FRP adhesive failure, (d) SRG fiber slipping, and (e) SRG mortar-brick detachment (Ghiassi et al., 2014).

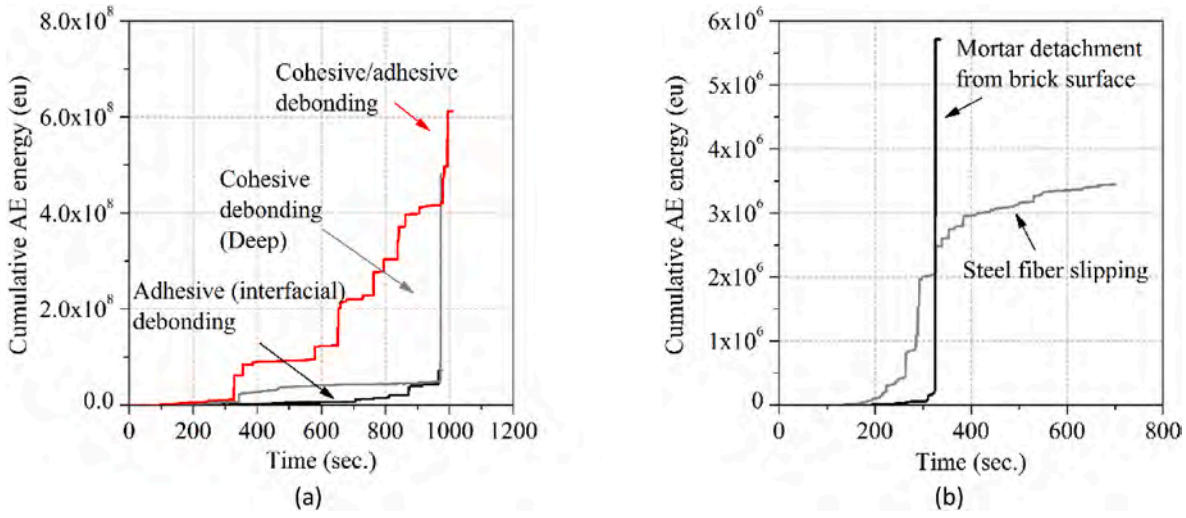


**Fig. 28.** (a) Representative results of cumulative AE energy measured during shear bond tests on brick specimens with FRP-strengthening and (b) SRG-strengthening (Verstrynge et al., 2016).

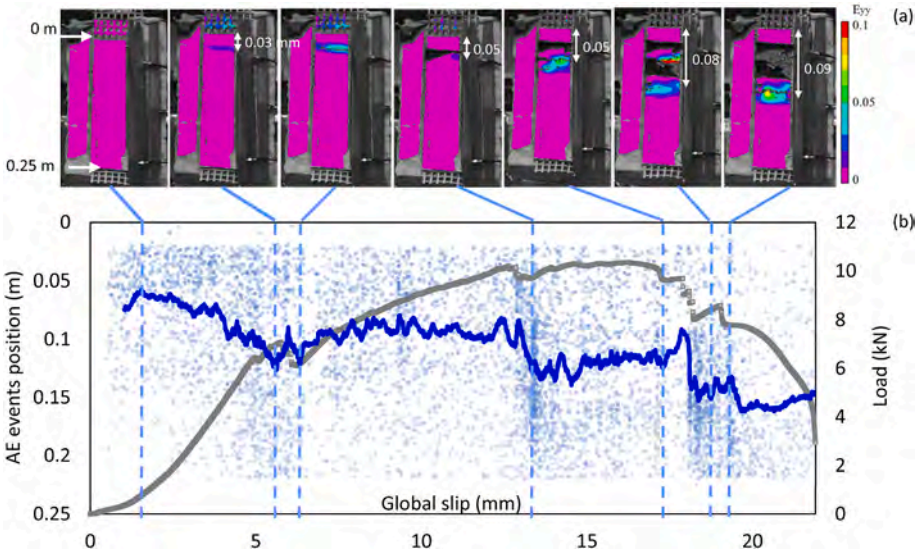


**Fig. 29.** Carbon TRC retrofit patch on masonry brick under single-lap shear test: (a) DIC Eyy strain maps, and (b) AE events localized in a vertical line along the TRC layer, as projected on the load-slip curve (Linn et al., 2022).

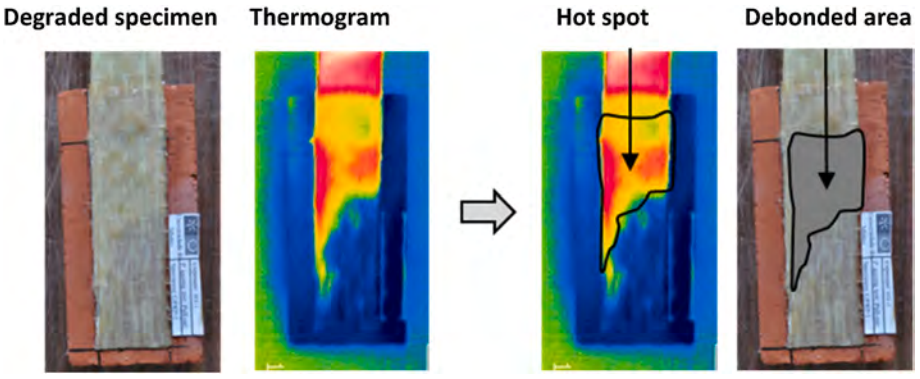


**Fig. 30.** Debonding detection with infrared thermography (Ghiassi et al., 2013; Verstrynge et al., 2016).

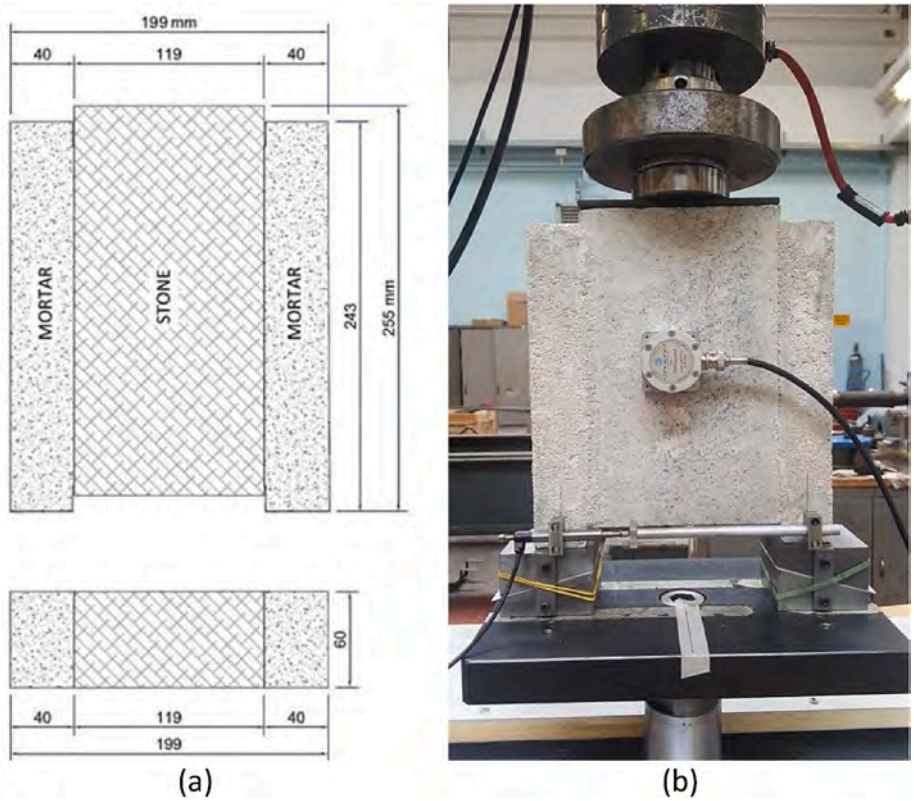


**Fig. 31.** (a) Side and top view of composite specimen, (b) test setup (Grazzini et al., 2020).

fracture process.

## 4. Industrial floor condition validated by impulse-response and impact-echo

Moving to a technique in the interphase between waves and vibrations, the following case includes the repair assessment of an industrial concrete floor. The floor was severely cracked, falling into the typology usually termed as "curling" (Kovler and Chernov, 2009), causing even problems in the driving of the vehicles. Repair through injection of grout through a primary grid was selected. Before and after the repair, the impulse response (I–R) technique was applied. In this case, a relatively high-intensity impact is inflicted on the test object (floor) using a load-cell instrumented hammer, that records the impact function. A geophone is attached next to the impact point in order to record the reaction of the member (Fig. 32(a)). When the material is very stiff or heavy, then the response (defined by the "mobility" curve), as calculated in the frequency domain through deconvolution of the impact and the recorded response, is expected to be low (Fig. 32(b)). However, when the top layer is delaminated, severely cracked or compromised in any way, a much higher mobility curve is expected (Fig. 32(b)). By applying the impact and reception on a regular pattern of points on the surface, a map can be created based on the average level or slope of the mobility curve indicating the current condition, while comparison before and after repair can highlight the improvement, as seen in Fig. 32(c) and (d). In this case, some points of higher mobility were persistent even after repair, leading to another injection round at a secondary grid. The I–R investigation (map in Fig. 32(d)) exhibited a much lower average level of mobility as well as revealed local changes in the areas of interest, verifying that the floor was adequately repaired (Zoidis et al., 2013).

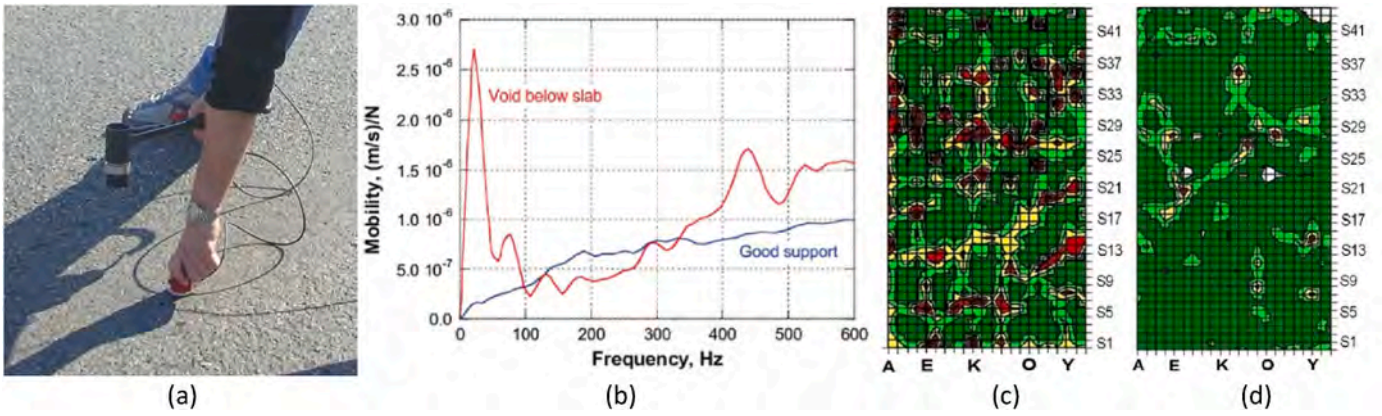


**Fig. 32.** (a) Impact hammering and geophone placement during I–R measurement, (b) indicative mobility curves (Germann Instruments, 2024), (c) mobility map before and (d) after grout injection on the concrete floor (Zoidis et al., 2013).

In other similar studies, the impact-echo method was applied in lab tests to assess the frequency corresponding to the highest amplitude peak for a series of concrete samples repaired by polymer cement mortar and tested in pull-off aiming at assessing the repair efficacy (Czarnecki et al., 2020, 2021). This parameter exhibited limited correlation to the results of the pull-off test, but proved very important for the detection of delaminations in the floor (Hola et al., 2011). As demonstrated in the studies, delamination of repaired floor structural elements could be adequately determined by examining the change of mobility curve. After determining the position of the potential defect, specific impact-echo measurements, based on the multiple reflections between the surface and the delaminated area, allowed extraction of the delamination depth. Taking both impact-echo frequency response and impulse response dynamic stiffness as input parameters for an artificial neural network numerical analysis, for the first time in the literature, the pull-off adhesion between the layers can be accurately evaluated. The actual pull-off strength exhibits deviations of less than 10% compared to the predicted values based on the NDT methodology comprising impulse-response, impact echo and their analysis through neural networks. It is emphasized that the prediction capability is greatly enhanced by combining the parameters in the neural network approach, while individual application of the techniques would not yield similarly successful results. In fact, a combination of different techniques is more promising than individual applications, while machine learning algorithms are gaining more space in the evaluation of repair (Szymanowski 2019).

## 5. Discussion

The cases mentioned above reveal that although various NDT techniques have well been used for damage characterization of different material and structure types, there is still much space for improvement in rationalizing their implementation in the field of repair/healing. Techniques based on elastic waves have the advantage of being sensitive to the stiffness of the media. Therefore, they are suitable to identify voids or cracks by the drop of the wave velocity and transmission. Reasonably, they work inversely and register a recovery when the cracks are closed by repair or self-healing. This has been clearly demonstrated in real structures, like bridges and dams, allowing a reliable assessment of the repair effectiveness. Though the primary information of the transit time is predominant, it is also argued that frequency could be manipulated in favor of characterization if conditions allow. The AE technique has also been helpful since repair bonds the crack sides and changes the overall material behavior under stress, providing changes to specific AE indices that clearly indicate the effectiveness of repair on-site and in the laboratory. Some other studies on AE, deal indirectly with the evaluation of repair and mainly with the compatibility of the repair/reinforcing layer to the substrate and the bonding conditions. Other techniques based on elastic waves, like the impulse-response and impact-echo, show quite evidently the improvement due to repair. Recently, electrical resistivity was assessed in terms of its capacity to determine or quantify the healing in concrete walls with vascular networks to supply self-healing agents. While resistivity consistently showed increased values after healing, it also exhibited strong fluctuations and sensitivity to moisture, factors that should be controlled to apply the technique in situ (Van Mullem et al., 2023). From the above review, it is apparent that elastic wave techniques form the majority of the available cases, certainly in situ, but also in the laboratory. This is the consequence of their ease of application, and the fact that their sensitivity to voids and discontinuities is far greater than their sensitivity to conditions like moisture and temperature. Simulations also show usefulness due to the specificities of the different cases and help to interpret the measured parameters in terms of the healing material properties. The critical point about NDT approaches is that, apart from qualitative information, they can offer a way to quantify the result in terms of well-established parameters like the UPV or mechanical properties like the elastic modulus. Therefore, they give information on the actual "healing" or repair in the sense of restoration of mechanical properties apart from simple "filling" of the discontinuities. This will lead to more reliable results, creating a basis for engineering decisions about the operation of the structure.

## 6. Conclusions

The issue of repair and evaluation of its effectiveness is of primary importance in the engineering world. However, so far, the repair has usually not been evaluated or was only evaluated by experience. In case robust methodologies can be established, characterization would be based on engineering criteria, increasing the confidence and the possibilities of acceptable performance after the end of repair works. NDT of repair is not widespread, while published studies are limited and scattered based on diverse applications. Non-destructive monitoring is a field that can offer much to the characterization of repair in civil engineering structures. Several meaningful research efforts have emerged showing the suitability of NDT techniques to evaluate the outcome of different repair methodologies. Parameters like bonding of external patches, restoration of stiffness due to repair material injection or closing of cracks due to self-healing can be well evaluated in the laboratory, while several applications are noted on a larger scale in-situ. However, these efforts are case-specific so far, meaning that geometries, sensors, and coupling types vary strongly. The present document aims to fill this gap in the literature and serves as a summary of the non-destructive inspection techniques to evaluate repair. The different techniques are presented in terms of their possibility of helping in the evaluation of repair as well as initial damage evaluation. The principles behind the techniques are briefly discussed and specific applications are also presented either in-situ on a real scale (dams, bridges, walls), or in the laboratory as promising evaluation techniques under development. This is one of the topics of RILEM technical committee 269-IAM and intends to act as a starting point for a broader discussion on research and implementation of evaluation of repair in civil engineering.

## CRediT authorship contribution statement

**T. Shiotani:** Writing – review & editing, Methodology, Conceptualization. **N. Ogura:** Writing – original draft, Validation, Supervision. **N. Okude:** Writing – original draft, Visualization, Investigation. **K. Watabe:** Writing – original draft, Methodology, Formal analysis. **C. Van Steen:** Writing – review & editing, Writing – original draft, Investigation. **E. Tsangouri:** Writing – review & editing, Writing – original draft, Supervision. **G. Lacidogna:** Writing – original draft, Supervision, Conceptualization. **S. Czarnecki:** Writing – original draft, Supervision, Methodology. **H.K. Chai:** Writing – original draft, Visualization, Conceptualization. **Y. Yang:** Writing – original draft, Supervision, Formal analysis. **E. Verstrynge:** Writing – review & editing, Writing – original draft, Supervision. **D.G. Aggelis:** Writing – review & editing, Writing – original draft, Project administration.

## Declaration of competing interest

The authors declare that they have no known competing financial interests or personal relationships that could have appeared to influence the work reported in this paper.

## Data availability

No data was used for the research described in the article.

## References


Aggelis, D.G., Shiotani, T., 2007. Repair evaluation of concrete cracks using surface and through-transmission wave measurements. Cement Concr. Compos. 29 (9), 700–711. https://doi.org/10.1016/j.cemconcomp.2007.05.001.

Aggelis, D.G., Shiotani, T., 2009. Experimental study of wave propagation through grouted concrete. ACI Mater. J. 106 (1), 19–24.

Aggelis, D.G., Shiotani, T., Polyzos, D., 2009. Characterization of surface crack depth and repair evaluation using Rayleigh waves. Cement Concr. Compos. 31 (1), 77–83. https://doi.org/10.1016/j.cemconcomp.2008.09.008.

Aggelis, D.G., Verbruggen, S., Tsangouri, E., Tysmans, T., Van Hemelrijck, D., 2013. Characterization of mechanical performance of concrete beams with external reinforcement by acoustic emission and digital image correlation. Construct. Build. Mater. 47, 1037–1045. https://doi.org/10.1016/j.conbuildmat.2013.06.005.

Aggelis, D.G., Verbruggen, S., Tsangouri, E., Tysmans, T., Van Hemelrijck, D., 2016. Monitoring the failure mechanisms of a reinforced concrete beam strengthened by textile reinforced cement using acoustic emission and digital image correlation. Smart Struct. Syst. 17 (1), 91–105. https://doi.org/10.12989/sss.2016.17.1.091.

Ahn, E., Kim, H., Sim, S., Shin, S., Shin, M., 2017. Principles and applications of ultrasonic-based nondestructive methods for self-healing in cementitious materials. Materials 10 (3), 278. https://doi.org/10.3390/ma10030278.

Aldea, C.M., Song, W.J., Popovics, J.S., Shah, S.P., 2000. Extent of healing of cracked normal strength concrete. J. Mater. Civ. Eng. 12 (1), 92–96.

Anzani, A., Binda, L., Carpinteri, A., Lacidogna, G., Manuello, A., 2008. Evaluation of the repair on multiple leaf stone masonry by acoustic emission. Mater. Struct. 41, 1169–1189. https://doi.org/10.1617/s11527-007-9316-z.

Bocca, P.G., Valente, S., Grazzini, A., Alberto, A., 2014. Detachment analysis of dehumidified repair mortars applied to historical masonry walls. Int. J. Architect. Herit. 8 (3), 336–348. https://doi.org/10.1080/15583058.2013.826304.

Carino, N., Stress Wave Propagation Methods, 2003. Chapter 14. In: Handbook on Nondestructive Testing of Concrete, second ed. CRC Press.

Carpinteri, A., Lacidogna, G., Puzzi, S., 2009. From criticality to final collapse: evolution of the b-value from 1.5 to 1.0. Chaos, Solit. Fractals 41 (2), 843–853. https://doi.org/10.1016/j.chaos.2008.04.010.

Carpinteri, A., Lacidogna, G., Manuello, A., 2011. The b-value analysis for the stability investigation of the ancient Athena temple in Syracuse. Strain 47, 243–253. https://doi.org/10.1111/j.1475-1305.2008.00602.x.

Chaix, J.-F., Garnier, V., Corneloup, G., 2006. Ultrasonic wave propagation in heterogeneous solid media: theoretical analysis and experimental validation. Ultrasonics 44 (2), 200–210. https://doi.org/10.1016/j.ultras.2005.11.002.

Cheng, H., Zhang, F., Yang, Y., Blom, C.B., Kees, .M., 2022. Monitoring of repaired concrete floor in the maastunnel using smart aggregates, IABMAS 2022. In: 11th International Conference on Bridge Maintenance, Safety and Management, Barcelona, 11-15 July, 2022.

Czarnecki, S., Sadowski, Ł., Hoła, J., 2020. Artificial neural networks for non-destructive identification of the interlayer bonding between repair overlay and concrete substrate. Adv. Eng. Software 141, 102769. https://doi.org/10.1016/j.advengsoft.2020.102769.

Czarnecki, S., Sadowski, Ł., Hoła, J., 2021. Evaluation of interlayer bonding in layered composites based on non-destructive measurements and machine learning: comparative analysis of selected learning algorithms. Autom. ConStruct. 132, 103977 https://doi.org/10.1016/j.autcon.2021.103977.

Delatte, N., 2009. Introduction chapter. In: Delatte, Norbert (Ed.), Failure, Distress and Repair of Concrete Structures. Woodhead Publishing xiii-xv.

El Kadi, M., Blom, J., Wastiels, J., Aggelis, D.G., 2017. Use of early acoustic emission to evaluate the structural condition and self-healing performance of textile reinforced cements. Mech. Res. Commun. 81, 26–31. https://doi.org/10.1016/j.mechrescom.2017.02.007.

Feng, Q., Cui, J., Wang, Q., Fan, S., Kong, Q., 2018. A feasibility study on real-time evaluation of concrete surface crack repairing using embedded piezoceramic transducers. Measurement 122, 591–596. https://doi.org/10.1016/j.measurement.2017.09.015.

Fowler, T.J., 1977. Acoustic Emission Testing of Fiber Reinforced Plastics, ASCE Fall Convention, San Francisco.

German Instruments, 2024 https://www.germanninstruments.com/impulse-response-test-smash/(accessed March 2024).

Ghiassi, B., Silva, S.M., Oliveira, D.V., Lourenço, P.B., Bragança, L., 2013. Assessment of the Bond Quality in FRP-Strengthened Masonry Using IR Thermography Technique, FRPRCS-11. Giumarães, Portugal.

Ghiassi, B., Verstrynge, E., Lourenco, P.B., Oliveira, D.V., 2014. Characterization of debonding in FRP-strengthened masonry using the acoustic emission technique. Eng. Struct. 66, 24–34. https://doi.org/10.1016/j.engstruct.2014.01.050.

Grazzini, A., Lacidogna, G., 2021. Mechanical properties of historic masonry stones obtained by in situ non-destructive tests on the st. Agostino church in amatrice (Italy). Appl. Sci. 11 (14), 6352. https://doi.org/10.3390/app11146352.

Global Structural Health Monitoring Market Size, Share, and COVID-19 Impact Analysis, Spherical Insights, 2021, 160, Grazzini, A., Accornero, F., Lacidogna, G., Valente, S., 2020. Acoustic emission and numerical analysis of the delamination process in repair plasters applied to historical walls. Construct. Build. Mater. 236 https://doi.org/10.1016/j.conbuildmat.2019.117798.

Grosse, C.U., Ohtsu, M., Aggelis, D.G., Shiotani, T. (Eds.), 2022. Acoustic Emission Testing. Springer. https://doi.org/10.1007/978-3-030-67936-1.

Hola, J., Sadowski, L., Schabowicz, K., 2011. Nondestructive identification of delaminations in concrete floor toppings with acoustic methods. Autom. ConStruct. 20 (7), 799–807. https://doi.org/10.1016/j.autcon.2011.02.002.

Issa, C.A., 2009. Methods of crack repair in concrete structures, Chapter 6. In: Delatte, Norbert (Ed.), Failure, Distress and Repair of Concrete Structures. Woodhead Publishing.

Jacobs, L.J., Owino, J.O., 2000. Effect of aggregate size on attenuation of Rayleigh surface waves in cement-based materials. J. Eng. Mech. 126 (11), 1124–1130.

Jacobsen, S., Marchand, J., Hornain, H., 1995. SEM observations of the microstructure of frost deteriorated and self-healed concretes. Cement Concr. Res. 25 (8), 1781–1790. https://doi.org/10.1016/0008-8846(95)00174-3.

Jacobsen, S., Marchand, J., Boisvert, L., 1996. Effect of cracking and healing on chloride transport in OPC concrete. Cement Concr. Res. 26 (6), 869–881. https://doi.org/10.1016/0008-8846(96)00072-5.

Kaur, N.P., Shah, J.K., Majhi, S., Mukherjee, A., 2019. Healing and simultaneous ultrasonic monitoring of cracks in concrete. Mater. Today Commun. 18, 87–99. https://doi.org/10.1016/j.mtcomm.2018.10.022.

Kaur, N.P., Majhi, S., Dhami, N.K., Mukherjee, A., 2020. Healing fine cracks in concrete with bacterial cement for an advanced non-destructive monitoring. Construct. Build. Mater. 242, 118151 https://doi.org/10.1016/j.conbuildmat.2020.118151.

Kobayashi, Y., Shiotani, T., 2016. Computerized AE tomography. RILEM State-of-the-Art Reports 20, 47–68.

Kovler, K., Chernov, V., 2009. Types of damage in concrete structures, Chapter 2. In: Failure, Distress and Repair of Concrete Structures. Norbert Delatte, Woodhead Publishing, pp. 32–56.

Kwaśniewski, L., Garbacz, A., 2008. Characterization of Stress Wave Propagation in Impact-Echo Method Using FEM Models of Repair Systems, Challenges for Civil Construction. FEUP, Porto, pp. 92–93. CD.

Lefever, G., Snoeck, D., De Belie, N., Van Vlierberghe, S., Van Hemelrijck, D., Aggelis, D. G., 2020. The contribution of elastic wave NDT to the characterization of modern cementitious media. Sensors 20 (10), 2959. https://doi.org/10.3390/s20102959.

Lefever, G., Van Hemelrijck, D., Snoeck, D., Aggelis, D.G., 2022a. Self-healing assessment of cementitious mortars through ultrasonic monitoring. Cement Concr. Compos. 133, 104683 https://doi.org/10.1016/j.cemconcomp.2022.104683.

Lefever, G., Van Hemelrijck, D., Aggelis, D.G., Snoeck, D., 2022b. Evaluation of self-healing in cementitious materials with superabsorbent polymers through ultrasonic mapping. Construct. Build. Mater. 344, 128272 https://doi.org/10.1016/j.conbuildmat.2022.128272.

Lefever, G., Abdullah, A., Van Hemelrijck, D., Snoeck, D., Aggelis, D.G., 2024. Air-coupled ultrasonic mapping of stimulated autogenous self-healing and repair effectiveness within concrete mixtures. Construct. Build. Mater. 419, 135547 https://doi.org/10.1016/j.conbuildmat.2024.135547.

Linn, D.M., Aggelis, D.G., Tsangouri, E., 2022. Single-lap shear tests of textile reinforced mortar retrofit systems bonded to masonry: revealing the fracture progress by digital image correlation and acoustic emission. Mater. Struct. 55 (7) https://doi.org/10.1617/s11527-021-01850-3.

Mahmoud, A.M., Ammar, H.H., Mukdadi, O.M., Ray, I., Imani, F.S., Chen, A., Davalos, J. F., 2010. Non-destructive ultrasonic evaluation of CFRP–concrete specimens subjected to accelerated aging conditions. NDT E Int. 43 (7), 635–641. https://doi.org/10.1016/j.ndteint.2010.06.008.

Markets and Markets, 2024, https://www.marketsandmarkets.com/ResearchInsight/concrete-repair-mortar-market.asp, accessed February 2024.

Mohseni, H., Ng, C.T., 2019. Rayleigh wave propagation and scattering characteristics at debondings in fibre-reinforced polymer-retrofitted concrete structures. Struct. Health Monit. 18 (1), 303–317. https://doi.org/10.1177/1475921718754371.

Momoki, S., Shiotani, T., Chai, H.K., Aggelis, D.G., Kobayashi, Y., 2013. Large-scale evaluation of concrete repair by three-dimensional elastic-wave-based visualization technique. Struct. Health Monit. 12 (3), 240–251. https://doi.org/10.1177/1475921713479640.

Muhammad, N.Z., Shafaghat, A., Keyvanfar, A., Majid, M.Z.A., Ghoshal, S.K., Yasouj, S.E. M., Ganiyu, A.A., Kouchaksaraei, M.S., Kamyab, H., Taheri, M.M., Shirdar, M.R., 2016. Tests and methods of evaluating the self-healing efficiency of concrete: a review. Construct. Build. Mater. 112, 1123–1132. https://doi.org/10.1016/j.conbuildmat.2016.03.017.

Naik, T., Malhotra, V., Popovics, J., 2003. The ultrasonic pulse velocity method. In: Handbook on Nondestructive Testing of Concrete, second ed. CRC Press (Chapter 8).

Ogura, N., Konishi, Y., Sagradyan, A., Shiotani, T., 2023. Monitoring of repaired water leaks using surface wave tomography. Developments in the Built Environment 14, 100133. https://doi.org/10.1016/j.dibe.2023.100133.

Okude, N., Shiotani, T., Nishida, T., Furuno, Syogo, 2018. Evaluation of crack repair effect for RC slab using AE Tomography. PROGRESS in ACOUSTIC EMISSION XIX, 127–132.

Papasergio, A.E., Ugolotti, G., Lessio, M., Sassoni, E., 2023. New insights on conservation of marble artworks from computational chemistry. Mater. Today: Proc. https://doi.org/10.1016/j.matpr.2023.06.467.

RILEM TC 269-IAM, 2023. https://www.rilem.net/groupe/269-iam-damage-assessment-in-consideration-of-repair-retrofit-recovery-in-concrete-and-masonry-structures-by-means-of-innovative-ndt-347.

Sagradyan, A., Ogura, N., Shiotani, T., 2023. Application of elastic wave tomography method for damage evaluation in a large-scale reinforced concrete structure. Developments in the Built Environment 14, 100127. https://doi.org/10.1016/j.dibe.2023.100127.

Şahmaran, M., Keskin, S.B., Ozerkan, G., Yaman, I.O., 2008. Self-healing of mechanically-loaded self consolidating concretes with high volumes of fly ash. Cement Concr. Compos. 30 (10), 872–879. https://doi.org/10.1016/j.cemconcomp.2008.07.001.

Saidi, M., Reboul, N., Gabor, A., 2022. Analysis of bond behaviour of textile-reinforced cement (TRC) applied to masonry using distributed fibre optic sensors and acoustic

emission. Compos. B Eng. 247, 110327 https://doi.org/10.1016/j.compositesb.2022.110327.
Santos, P., Júlio, E., Santos, J., 2010. Towards the development of an in situ non-destructive method to control the quality of concrete-to-concrete interfaces. Eng. Struct. 32 (1), 207–217. https://doi.org/10.1016/j.engstruct.2009.09.007.
Shiotani, T., Aggelis, D.G., 2007. Evaluation of repair effect for deteriorated concrete piers of intake dam using AE activity. J. Acoust. Emiss. 25, 69–79.
Shiotani, T., Momoki, S., Chai, H.K., Aggelis, D.G., 2009. Elastic wave validation of large concrete structures repaired by means of cement grouting. Construct. Build. Mater. 23 (7), 2647–2652. https://doi.org/10.1016/j.conbuildmat.2009.01.005.
Silfwerbrand, J., 2009. Bonded Concrete Overlays for Repairing Concrete Structures, Chapter in Failure, Distress and Repair of Concrete Structures. Woodhead Publishing, pp. 208–243. https://doi.org/10.1533/9781845697037.2.208.
Song, G., Gu, H., Mo, Y.L., 2008. Smart aggregates: multi-functional sensors for concrete structures-a tutorial and a review. Smart Mater. Struct. 17 (3), 033001 https://doi.org/10.1088/0964-1726/17/3/033001.
Szymanowski, J., 2019. Evaluation of the adhesion between overlays and substrates in concrete floors: literature survey, recent non-destructive and semi-destructive testing methods, and research gaps. Buildings 9, 203. https://doi.org/10.3390/buildings9090203.
Takamine, H., Watabe, K., Miyata, H., Asaue, H., Nishida, T., Shiotani, T., 2018. Efficient damage inspection of deteriorated RC bridge deck with rain-induced elastic wave. Construct. Build. Mater. 162, 908–913.
Tsangouri, E., Aggelis, D.G., Van Tittelboom, K., De Belie, N., Van Hemelrijck, D., 2013. Detecting the activation of a self-healing mechanism in concrete by acoustic emission and digital image correlation. Sci. World J. 2013, 424560 https://doi.org/10.1155/2013/424560.
Tsangouri, E., Karaiskos, G., Aggelis, D.G., Deraemaeker, A., Van Hemelrijck, D., 2015. Crack sealing and damage recovery monitoring of a concrete healing system using embedded piezoelectric transducers. Struct. Health Monit. 14 (5), 462–474. https://doi.org/10.1177/1475921715596219.
Tsangouri, E., Aggelis, D.G., Matikas, T.E., Mpalaskas, A.C., 2016. Acoustic emission activity for characterizing fracture of marble under bending. Appl. Sci. 6 (1) https://doi.org/10.3390/app6010006.
Tsangouri, E., Lelon, J., Minnebo, P., Asaue, H., Shiotani, T., Van Tittelboom, K., De Belie, N., Aggelis, D.G., Van Hemelrijck, D., 2019. Feasibility study on real-scale, self-healing concrete slab by developing a smart capsules network and assessed by a plethora of advanced monitoring techniques. Construct. Build. Mater. 228, 116780 https://doi.org/10.1016/j.conbuildmat.2019.116780.
Tsangouri, E., Van Loo, C., Shields, Y., De Belie, N., Van Tittelboom, K., Aggelis, D.G., 2022. Reservoir-vascular tubes network for self-healing concrete: performance analysis by acoustic emission, digital image correlation and ultrasound velocity. Appl. Sci. 12 (10), 4821. https://doi.org/10.3390/app12104821.
Van Mullem, T., Lefever, G., Decuypere, A., De Vleeschouwer, E., Shields, Y., De Brabandere, L., Snoeck, D., Aggelis, D.G., De, Belie N., 2023. Preliminary analysis of non-destructive test methods to evaluate the self-healing efficiency on the construction site. In: International RILEM Conference on Synergising Expertise towards Sustainability and Robustness of Cement-Based Materials and Concrete Structures. SynerCrete 2023, vol. 43. RILEM Bookseries. https://doi.org/10.1007/978-3-031-33211-1_33. Springer, Cham.
Van Tittelboom, K., De Belie, N., Lehmann, F., Grosse, C.U., 2012. Acoustic emission analysis for the quantification of autonomous crack healing in concrete. Construct. Build. Mater. 28 (1), 333–341. https://doi.org/10.1016/j.conbuildmat.2011.08.079.
Vangansbeke, E., Shields, Y., De Belie, N., Van Tittelboom, K., Tsangouri, E., 2023. Autonomous healing by vascular networks: tracking of cracks interaction by Ultrasounds and Acoustic Emission. In: MATEC Web of Conferences, vol. 378. EDP Sciences, 04003. https://doi.org/10.1051/matecconf/202337804003.
Verstrynge, E., Wevers, M., Ghiassi, B., Lourenço, P.B., 2016. Debonding damage analysis in composite-masonry strengthening systems with polymer- and mortar-based matrix by means of the acoustic emission technique. Smart Mater. Struct. 25 (1), 015009 https://doi.org/10.1088/0964-1726/25/1/015009.
Wang, B., Gupta, R., 2021. Analyzing bond-deterioration during freeze-thaw exposure in cement-based repairs using non-destructive methods. Cement Concr. Compos. 115, 103830 https://doi.org/10.1016/j.cemconcomp.2020.103830.
Zhang, H., Li, J., Kang, F., Zhang, J., 2022. Monitoring and evaluation of the repair quality of concrete cracks using piezoelectric smart aggregates. Construct. Build. Mater. 317, 125775 https://doi.org/10.1016/j.conbuildmat.2021.125775.
Zhong, W., Yao, W., 2008. Influence of damage degree on self-healing of concrete. Construct. Build. Mater. 22 (6), 1137–1142. https://doi.org/10.1016/j.conbuildmat.2007.02.006.
Zoidis, N., Tatsis, E., Vlachopoulos, C., Gotzamanis, A., Clausen, J.S., Aggelis, D.G., Matikas, T.E., 2013. Inspection, evaluation and repair monitoring of cracked concrete floor using NDT methods. Construct. Build. Mater. 48, 1302–1308. https://doi.org/10.1016/j.conbuildmat.2013.06.082.